

**PORE STRUCTURE INVESTIGATION OF MONOLITHIC CARBON
BLACK - SILICA AEROGEL COMPOSITES FOR HIGH
TEMPERATURE INSULATION APPLICATIONS**

by

Pınar Çetin

**A Thesis Submitted to the
Graduate School of Engineering
in Partial Fulfillment of the Requirements for
the Degree of**

Master of Science

in

Materials Science and Engineering

Koc University

August 2008

Koc University

Graduate School of Sciences and Engineering

This is to certify that I have examined this copy of a master's thesis by

Pınar Çetin

and have found that it is complete and satisfactory in all respects,
and that any and all revisions required by the final
examining committee have been made.

Committee Members:

Prof. Dr. Can Erkey (Advisor)

Prof. Dr. Alper Kiraz

Asst. Prof. A. Neren Ökte

Date:

ABSTRACT

The macroscopic properties of aerogels such as thermal, optical and mechanical are a result of the micro structures of these materials. In this thesis carbon black – silica composite aerogel materials were prepared with different carbon contents and the effects of carbon content on the pore properties and the micro structure of silica aerogels are reported which were not investigated in literature. Aerogels were synthesized by two step sol - gel method using TEOS (Tetraethylorthosilicate) as precursor, HCl and NH₄OH as catalysts, ethanol as solvent and dried by the supercritical CO₂ extraction method. The effects of TEOS concentration, gelation and aging temperature on pore properties of aerogels were investigated. Increasing TEOS concentration in the sol shifted the pore size distributions to smaller pore diameters with a sharper peak. The aerogels were aged in water-ethanol solutions at different temperatures which caused the pore volume to increase dramatically. Cabot Vulcan XC72R was used for the synthesis of carbon black-silica aerogel composites. The powder premixed with ethanol was added to the silica sol just before the gelation step. It was shown that addition of carbon black to the sol at different ratios did not affect the porous structure of the silica matrix covering the carbon black particles. By this method silica aerogels with a pore volume of 5.3cc/g and carbon black silica composite aerogels with a pore volume of 4.6cc/g and surface areas on the order of 1000 m²/g were synthesized.

ÖZET

Aerogellerin optik termal ve mekanik özellikler gibi makroskopik özellikleri malzemenin mikro yapısından ilri gelir. Bu özellikleri kontrol etmek çeşitli parametrelerin gözenek yapılarına olan etkilerini bilmek ile mümkün olur. Bu tezde karbon siyah – silika aerogel kompozit malzemeler değişik karbon siyah miktarları ile hazırlandı ve literatürde daha önce araştırılmamış olan kompozit yapımında kullanılan karbon siyah miktarının malzemelerin gözenek yapılarına etkileri rapor edildi. Monolitik silika aerogeller ve karbon siyah – silika aerogel kompozitler iki adımlı sol-jel metodu ile sentezlendi. Silika kaynağı olarak TEOS (teraethylorthosilicate), katalizör olarak HCl ve NH₄OH, çözücü olarak etanol kullanıldı ve kurutma süper kritik karbon dioksit ekstraksiyon yöntemi ile gerçekleştirildi. TEOS konsantrasyonunu, yaşlandırma solüsyonlarını ve yaşlandırma sıcaklıklarını da içeren çeşitli sol-jel parametrelerinin malzemenin gözenek özellikleri üzerindeki etkileri araştırıldı. TEOS konsantrasyonunu arttırmak gözenek boyutu dağılımlarını küçük gözenek çaplarına doğru daha sivri piklerle kaydırıldı. Alkojeller su-etanol solüsyonlarında değişik sıcaklıklarda yaşlandırıldı. Jellerin yaşlandırılması gözenek hacmini etkili bir biçimde arttırdı. Karbon siyah – silika kompozit aerogel sentezinde karbon siyah tozu olarak Cabot Vulcan XC72R kullanıldı. Etanol ile önceden karıştırılmış toz silika soluna tam jelleşme öncesi eklendi. Karbon siyah eklenmesinin karbon siyah parçacıklarını çevreleyen silika ağının gözenek yapısını etkilemediği görüldü. Bu yöntem ile yüzey alanları 1000m²/g seviyelerinde olan, gözenek hacmi 5.3cc/g olan silika aerogeller ve gözenek hacmi 4.6 olan karbon siyah - silika kompozit aerogeller sentezlendi.

ACKNOWLEDGEMENTS

I would like to express my gratitude to my supervisor Prof. Can Erkey who have been a great source of inspiration and provided his right balance of suggestions, criticism, and freedom.

I am grateful to members of my thesis committee for critical reading of this thesis and for their valuable comments.

I would like to thank TUBITAK (Grant 107M326) for the foundation of this project.

My colleagues supported me in my research work. I want to thank them for all their help, support, interest and valuable hints. I also would like to thank Seda Giray for her helps on characterization of pore structures.

Especially, I would like to give my special thanks to my family and friends for their patient love that enabled me to complete this work.

TABLE OF CONTENTS

List of Tables	vii
List of Figures	viii
Chapter 1: Introduction	1
1.1 Motivation.	1
1.2 Literature Review.	3
1.3 Objectives.	25
Chapter 2: Experimental	26
2.1 Synthesis	26
2.2 Aging Solutions and Temperatures.	30
2.3 Drying Apparatus and Conditions.	31
2.4 Preparation of Carbon black – Silica Aerogel Composite Materials.	33
2.5 Characterization Methods.	34
Chapter 3: Results and Discussions	44
3.1 TEOS Concentration Effect	44
3.2 Aging Effect	48
3.3 Carbon Black – Silica Aerogel Composites.	52
Chapter 4: Conclusions	63
Bibliography	65

LIST OF TABLES

Table 1.1 Thermal Conductivity of Various Materials	2
Table 2.1 Reactant amounts for one sample preparation	27
Table 2.2 The Carbon black amounts used in the synthesis of composite aerogels	33
Table 3.1. TEOS Concentration effect	45
Table 3.2 Effect of Aging Conditions	49
Table 3.3 Properties of carbon black - silica composite aerogels	53
Table 3.4 The densities and calculated pore volumes of silica aerogel samples after and before degas	56

LIST OF FIGURES

Figure 1.1 Ternary phase diagram of the system TEOS-ethanol-water at 298K	5
Figure 1.2 Dependence of the hydrolysis and condensation rates on the pH of the solution	6
Figure 1.3 The effect of Hydrolysis pH on the specific pore volume and specific surface area of silica aerogels produced with two step method	7
Figure 1.4 The effect of gelation pH on the specific pore volume and specific surface area of silica aerogels produced with two step method	8
Figure 1.5 Evolution of viscosity and shear modulus as a function of time, for a precursor solution undertaking polymeric gelation	9
Figure 1.6 Representation of a porous wet gel filled with pore liquid	12
Figure 1.7 High temperature supercritical drying with methanol	13
Figure 1.8 Low temperature supercritical drying with carbon dioxide	15
Figure 1.9 Illustration of the spring back effect	16
Figure 1.10 Schematic representation of the silation process	17
Figure 1.11 Variation of thermal conductivity of different opacified aerogel insulants at 300 K with air pressure	20
Figure. 1.12 Comparisons of effective thermal conductivities of polyurethane foam samples against the solid volume fraction in polyurethane foams	22
Figure 1.13 Measured and calculated total thermal conductivity depending on the temperature at 3.2 bar ($3.2 \cdot 10^5$ Pa) external load and a gas pressure of 100 Pa (1 mbar)	23
Figure 1.14 Calculated variation of thermal conductivity of opacified aerogels as a function of density, for temperatures 300, 400 and 500K	24

Figure 2.1 The schematic representation of the procedure during silica aerogel synthesis by sol-gel method	27
Figure 2.2 The pictures of the two molding systems used in this study. A: Teflon ring mold system and the syringe mold both loaded with sol solutions. B: Front view of the Teflon ring mold that is filled with 2ml sol solution. C: Opened flat mold with the gel on the glass plate	29
Figure 2.3 The pictures of two monolithic samples one flat mold and another cylindrical prepared from two different molds	30
Figure 2.4 A) Schematic representation of the supercritical extraction set-up. B) The image of the experimental apparatus for supercritical extraction	31
Figure 2.5 Preparation of carbon black silica aerogel composite in a beaker on a magnetic stirrer and the pictures of carbon black powder and a monolithic composite sample	33
Figure 2.6 The six types of adsorption isotherms classified by IUPAC	36
Figure 2.7 Adsorption process according to BET model and the the real model	38
Figure. 2.8 Schematic representation of multilayer adsorption, pore condensation in a single cylindrical pore	40
Figure 2.9 Relationship of $\frac{V}{V_0}$ and $\frac{r}{r_0}$ in a cylindrical pore	41
Figure 2.10 Transmission electron microscopy	42
Figure 3.1 Pore size distributions of aerogels with different TEOS concentrations	46
Figure 3.2 TEOS conc. effect on average pore size	46
Figure 3.3 Images of silica aerogels having different TEOS concentrations given as wt % to sol	47
Figure 3.4 TEOS conc. effect on pore volume	47
Figure 3.5 Pore size distributions of silica aerogels aged in different solvents	50

Figure 3.6 TGA results of 2 silica aerogel samples a) heat treated before TGA analysis, b)TGA analysis directly after drying	51
Figure 3.7 Pore size distributions of carbon-silica composite aerogels with different carbon contents	54
Figure 3.8 Carbon Wt % effect on pore volume of composite aerogels	54
Figure 3.9 Carbon Wt % effect on pore width of composite aerogels	55
Figure 3.10 Carbon Wt % effect on BET surface area of composite aerogels	55
Figure 3.11 Bright field TEM images obtained from the composite with 0.34 wt. % carbon	57
Figure 3.12 Bright field TEM images obtained from the composite with 4.50 wt. % carbon	58
Figure 3.13 High-resolution TEM images obtained from the composite with 4.50 wt. % carbon showing the structural detail in regions of: (a) silica aerogel; (b) carbon black	58
Figure 3.14 Infra-red transmittance spectra obtained from the carbon black - silica aerogel composites showing no effect of carbon content on oscillation modes	59
Figure 3.15 Raman spectra obtained from the carbon black - silica aerogel composites showing the emergence of the D (sp^3) and G (sp^3) band peaks with increasing carbon content	60

Chapter 1

INTRODUCTION

1.1 Motivation

Environmental concerns including global warming have become a driving force for researchers to find ways to decrease energy consumption in the world. Improving thermal insulation is a promising way of decreasing the energy consumption without reducing life standards. Development of advanced insulation materials is important for reducing high heat losses in buildings or in white goods. Particularly, an improvement in thermal insulation of oven windows with transparent silica aerogels and other parts of ovens, refrigerators or dryers with opacified composite aerogels can result in significant reduction of energy usage in houses. Silica aerogels are promising materials for thermal insulation of windows due to their low thermal conductivities and high transparencies among other insulation materials [1]. They exhibit thermal conductivities that are lower than 20 mW/Km^{\cdot} where air has a thermal conductivity of $24.1 \text{ mW/K}^{\cdot}\text{m}^{\cdot}$ under the same conditions [2]. Table 1.1 shows that using aerogels for thermal insulation can save two-three times more energy than other existing materials including chlorofluorocarbons having two-three times thermal conductivities [3]. For the other parts of buildings or white goods where transparency is not important but mechanical and thermal properties are critical, composite silica aerogels are very suitable having the advantage of lower thermal conductivities at high temperatures and better mechanical properties than silica aerogels.

Since silica aerogels were recognized with their exceptional properties they were found to be good candidates for many applications such as thermal insulation, electronic devices, filters, particle detectors and catalysts. As the scientists started to work to use aerogels for these applications they found out that it is possible to customize the aerogels for each specific application. The key parameter to control the physical properties of these materials for different applications is to control the pore structure of these materials. Fricke et al. and Hrubesh et al. showed the relation of thermal conductivity and pore properties [4-5]. Also it is known that transparency is directly related to the pore size distribution [6].

The radiative transport at low temperatures can be neglected because silica aerogels absorb heat sufficiently. However, in thermal insulation applications for high temperatures reduction of the radiative heat transport is essential. Carbon black having a broad absorption in that range is a very suitable opacifier. The opacified silica aerogels have a large potential to replace the conventional insulators such as polystyrene, polyurethane or fibers having extremely low thermal conductivities at high temperatures as well as low temperatures. Moreover opacified silica aerogels are non-combustible, are not hazardous for environment or human health and are easily disposed of.

Another drawback to use silica aerogels as monolithic blocks is that they are fragile and brittle. Composite aerogel is a promising way to overcome such disadvantages coming from the nature of the silica aerogel.

It is also important to be able to control the pore properties of the composite aerogels. The investigation of the effect of carbon black addition to the pore properties of the carbon black silica aerogels is reported in this thesis. This information will give light to predict the physical properties of the composite aerogels.

Table 1.1 Thermal Conductivity of Various Materials [3]

Materials	Thermal Conductivity (W/(m K))
Air	0.025
CCl ₂ F ₂	0.012
CCl ₃ F	0.007
Dense polyurethane	0.15
polyurethane foam	0.04
polyurethane foam with CFC	0.021
dense silica glass	1.00
silica powder	0.025
silica powder (evacuated)	0.004
silica aerogel	0.008
silica aerogel (evacuated)	0.002

1.2 Literature Review:

1.2.1 Monolithic and Transparent Silica Aerogels with Low Thermal Conductivities

Aerogels are synthesized by the [sol-gel process](#). Organic compounds containing silicon produce silicon dioxides (SiO_2) via chemical reactions. These silicon dioxide molecules form a three-dimensional network with each Si atom sharing four O atoms with the neighboring Si atom. As the chains grow the sol becomes more viscous and at some point it loses its fluidity and becomes a gel. This gel is composed of SiO_2 network with the solvent molecules in the pores. Using special drying techniques the solvent molecules are removed from the network leaving the pores filled with air. There have been many studies investigating how physical properties are affected by the nature of the catalysts and water amount in sol-gel polymerization [7-8].

1.2.1.1 Silica Aerogel Synthesis Using Different Precursors

Using sodium silicate: This method is the one that was used by Kistler, who has discovered the silica aerogels and known as the father of aerogels. The method uses water glass as the starting material and consists of four main steps.

1. Hydrogel preparation by the reaction of sodium silicate and hydrochloric acid.
2. The removal of sodium and chloride ions carefully.
3. Alcolgel production by extracting water in the hydrogel with alcohol.
4. Drying of the alcolgel over the critical point of the alcohol.

Aerogels produced using sodium silicate could not find many application areas because of the long and hard procedure. The time-consuming step is the removal of sodium and chloride ions with several washing cycles. It took more than 1 week to produce a small piece of aerogel.

Using tetraalkylsiloxanes: Teichner et al. [9] simplified the procedure using tetraalkylorthosilicates with a solvent that will be removed at supercritical conditions.

[Tetraalkylorthosilicates](#) The method using tetraalkylsiloxanes was published in 1966 [9]. Tetraethylorthosilicate (TEOS) is hydrolyzed and then gelled in the presence of water and hydrochloric acid in ethanol. Aerogel is then obtained after ethanol is removed at supercritical conditions. This method was improved in time and different tetraalkylorthosilicate precursors were used. The general formula for tetraalkylorthosilicate is $\text{Si}(\text{OR})_4$, where R is the alkyl

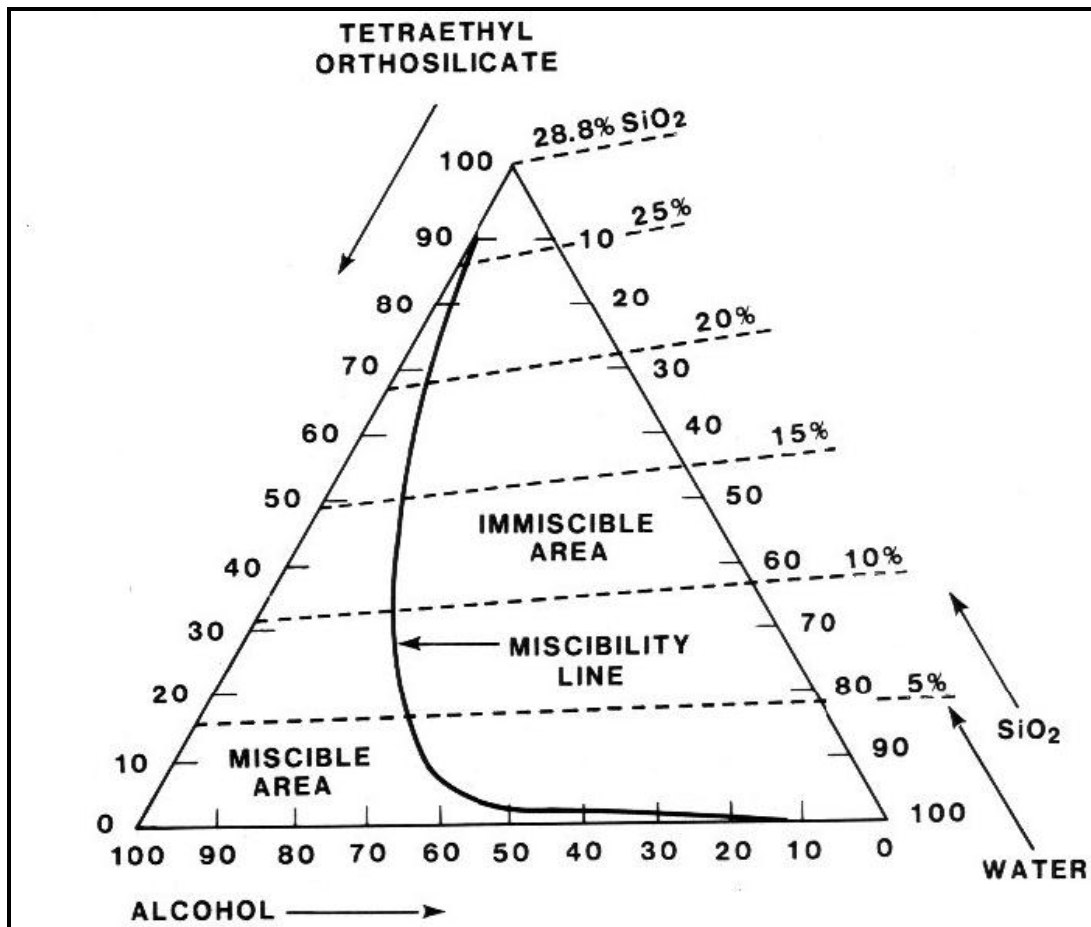


Figure 1.1 Ternary phase diagram of the system TEOS-ethanol-water at 298K [10].

Hydrolysis reaction:



Condensation reactions:

Alcohol condensation,



Water condensation,



Figure 1.2 shows that at acidic conditions hydrolysis reaction is favored. At first water is consumed during the hydrolysis reaction in acidic media; after that condensation reaction is favored by the addition of the base catalyst. After the first step, the solution contains many oligomers and polymers as a result of acid-catalyzed hydrolysis. In the second step in base media the polymers react or condense much faster than the monomers resulting in the growth of these polymers in various directions to form a cross-linked gel network.

There have been many studies on the effects of pH value and water amount on the properties of silica aerogels. Although the type of catalyst is important for the properties of the resulting aerogel, Karmarker showed that it is possible to perform hydrolysis reaction of TEOS with many kinds of acid catalysts regardless of the strength of the acid [13].

Increasing the water amount accelerates the hydrolysis reaction resulting in a lower gelation time. For condensation reactions, water is a by-product and the increasing water amount beyond a certain concentration shifts the equilibrium of the condensation reaction to the reactants. So it is another important parameter to be optimized. The water: $\text{Si}(\text{OR})_4$ ratio should be at least 2:1 in order to obtain enough hydrolyzed precursors for condensation reactions to reach gelation point. For molar ratios up to 6:1, alcohol condensation dominates, but at higher H_2O concentrations water condensation dominates [14]. Since water amount affects the rates of the reactions, it affects the particle size, pore volume and surface area of aerogels. In 1999 Stolarski reported that surface area and pore volume values are affected with the water amount. The highest surface area and pore volumes were obtained with a stoichiometric amount of water [15].

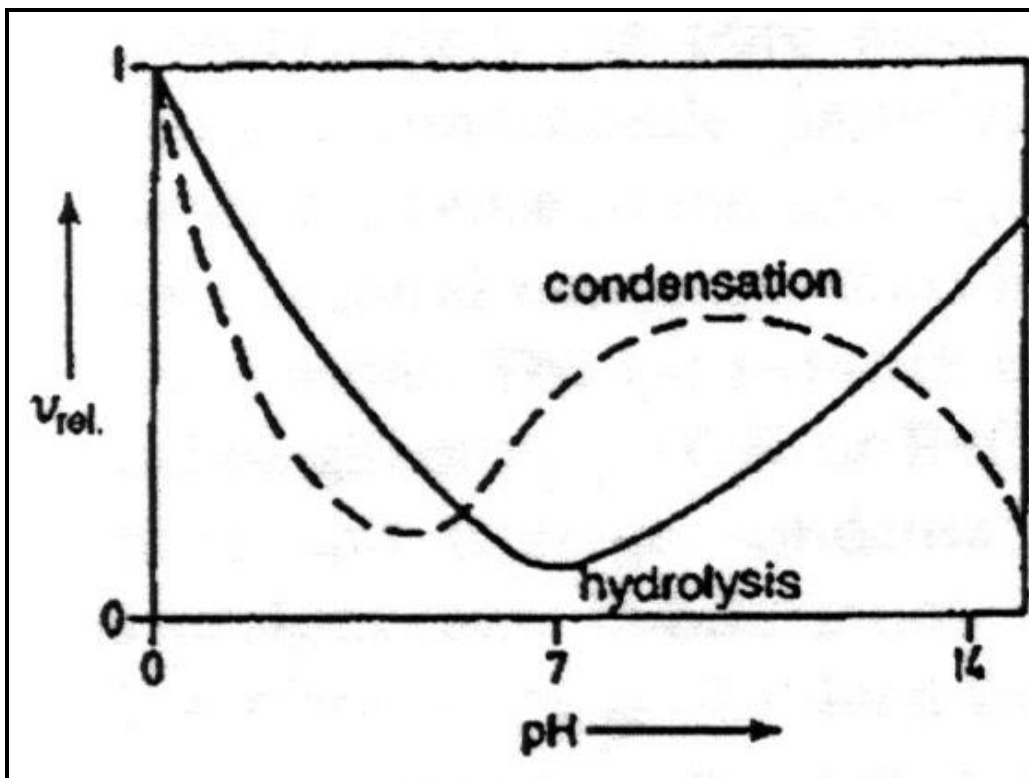


Figure 1.2 Dependence of the hydrolysis and condensation rates on the pH of the solution [12].

Stolarski's group also studied the effect of pH on both steps and some results are given in figures 1.3 and 1.4. They found out that when pH is less than 2, hydrolysis rate is very high and there are many uncondensed monomers that are available for further condensation reactions in the second step. Condensation of these monomers occurs very quickly and forms large 3-D structures which have very large volumes. When pH is increased in hydrolysis step, the rate decreases but at the end of the first step a partially condensed product is obtained. When pH is higher than 2.4, siloxane is dissolved and new monomers form which results in a more branched structure. The pore characterization data with respect to pH values shown in figure 1.3 indicate the increase in the pore volume and the decrease in the specific surface areas after the pH 2.4. In the case of condensation conditions the maximum pore volume and specific surface area values were obtained at pH 7.7 which is also believed to cause the highest condensation and redistribution rates [15].

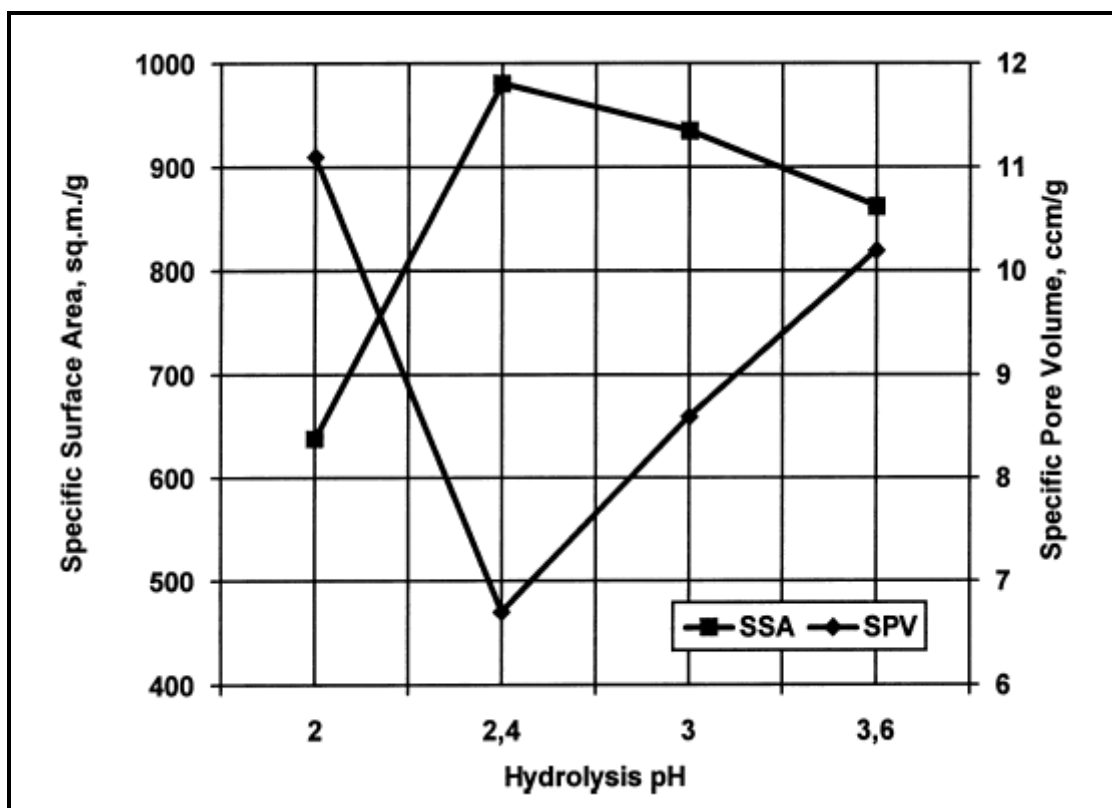


Figure 1.3 The effect of hydrolysis pH on the specific pore volume and specific surface area of silica aerogels produced with two step method [15].

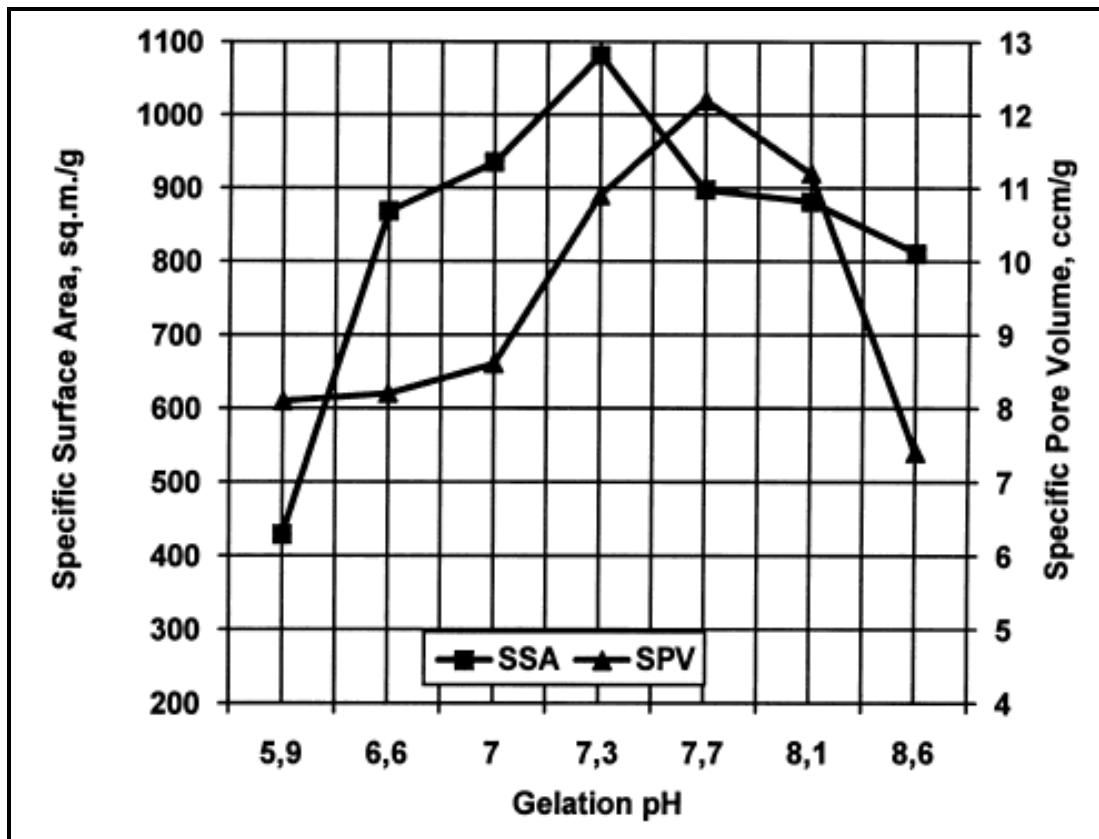


Figure 1.4 The effect of gelation pH on the specific pore volume and specific surface area of silica aerogels produced with two step method [15].

1.2.1.2 Aging

The gelation point is the moment when the last bond is formed in the network which makes the sol to lose its fluid character and turns it to an elastic solvent. At the gelation point, the chemical reactions do not finish and they continue during the process called aging. The structural changes that occur during aging have an important effect on the drying process. Figure 1.5 represents the changes in viscosity and shear modulus during sol gel processing. After the gelation point, shear modulus further increases with time. Aging affects the micro structure of the wet gel and so it changes the strength of the wet gel which is important during drying step to have a highly porous structure.

There are two different mechanisms that might occur during aging. One of them is the growth of the neck as a result of silica particles dissolving from particle surfaces and precipitating onto the necks. The second possibility is that the small particles dissolve and precipitate onto larger ones. The driving force for the material transport is difference in solubility, S , for surfaces with different curvatures, r , given by the Kelvin equation (1.1).

$$S_r = S_0 \exp\left(\frac{2\gamma_{sl}}{rV_m}\right) \quad (1.1)$$

where S_0 is the solubility of a flat surface of the solid phase, γ_{sl} is the solid-liquid interfacial energy, V_m is the molar volume of the solid, R is the ideal gas constant, and T is the temperature. All these parameters are constant for small or larger particles except for the curvature. Necks between particles have a negative curvature ($r < 0$) and hence a low solubility. Material will be transformed from concave surfaces of the particle and accumulate in these convex areas. The smaller particles have larger solubility. So, the driving force will also act to dissolve the smallest particles followed by precipitation onto larger particles.

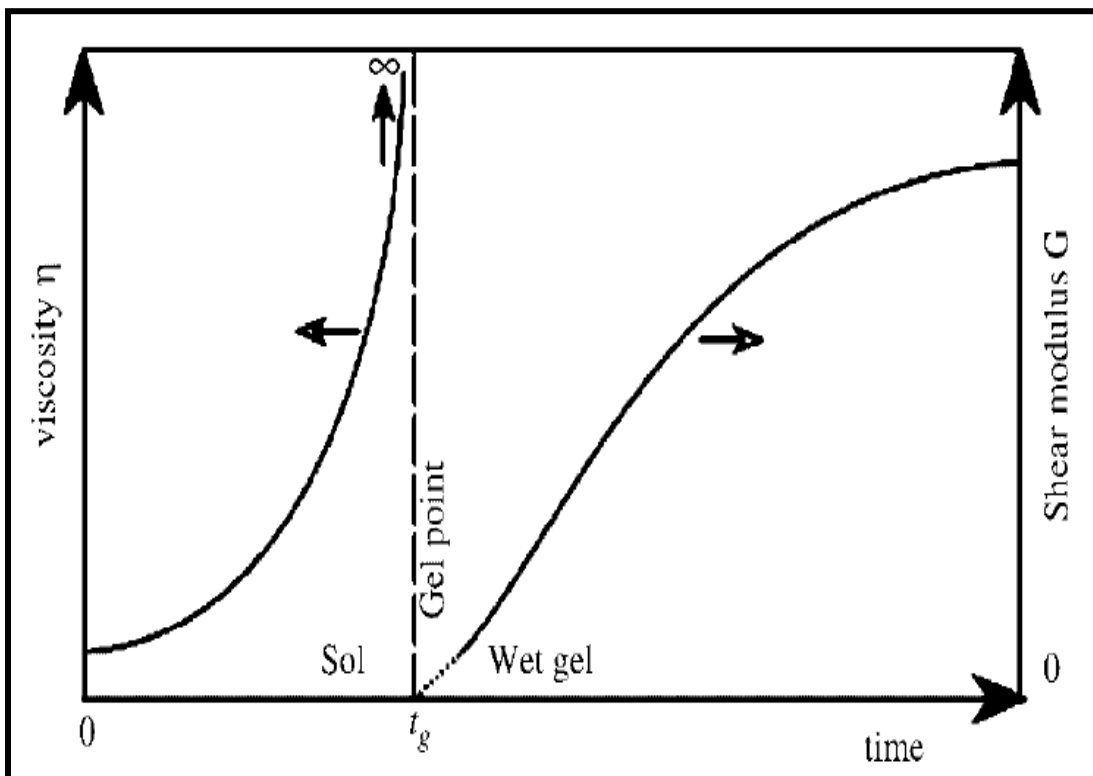


Figure 1.5 Evolution of viscosity and shear modulus as a function of time, for a precursor solution undertaking polymeric gelation [16].

S. Smitha et al. used TEOS solutions for investigating the effect of concentration of the aging solution and aging duration on the specific surface area, pore size and pore volume [17]. They report that increasing TEOS concentration in aging solutions increases the pore volume and specific surface area and aging time also has a similar effect on bulk density, surface area and pore volume. They obtained aerogels having a surface area of 1098 m²/g,

pore volume $1.31 \text{ cm}^3/\text{g}$ and an average pore size of 47.7 \AA by aging the wet gels in an 0 TEOS solution for 48 hr. It is reported that there is an optimum time of aging above which it has some negative effect on the porosity of the silica gel.

Juncal Estella et al. used ethanol or NH_3 (aq) (0.5 M and 2.0 M) as aging solutions for both xerogels and aerogels [18]. They reported that xerogels aged in ethanol were microporous whereas the ones aged in base media were mesoporous. When they dried the gels in supercritical conditions they obtained macroporous aerogels regardless of the aging media.

The studies of Arnaud Rigacci et al. showed that using water/ethanol and water/polyethoxydisiloxane as aging solutions enhanced both the permeability and mechanical properties of the wet gels [19]. It was also reported that there existed a pore-size distribution gradient between the surface and the bulk of the gel after aging of thick gels. In 2004 they attempted to solve this problem and aged the gels in less-concentrated polyethoxydisiloxane solutions. The resulting gels had a more homogeneous pore-size distribution. The same year G. Reichenauer et al. published a paper which is about the thermal aging of the gels in water [20]. They reported that the change in microporosity and surface groups of the wet gels during aging are key factors affecting shrinkage in supercritical drying.

1.2.1.3 Drying

The pores and the pore liquid in a wet gel can be represented as in figure 1.6. It is not a simple procedure to get rid of the pore liquid while conserving the nano-sized pores. While drying these gels in order to get a porous material, capillary forces have to be taken into consideration.

During the drying stage, capillary tension P_c is developed in the pore fluid by the creation of liquid-vapor menisci. The curvature of the meniscus r_m , which governs the magnitude of P_c , is related to the relative pressure P/P_0 of the pore fluid in the overlying gas by the Kelvin equation expressed in Eq. (1.2) [21],

$$P/P_0 = -2\gamma_{lv}/P_0 r_m = -2V_m R_g T / r_m \ln(P/P_0) \quad (1.2)$$

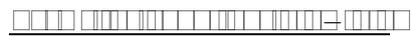
where V_m is the liquid molar volume, γ_{lv} is the pore fluid/ vapor surface tension, R_g is the gas constant and T is temperature. The maximum tension that can be developed in a pore of radius r_p is given by the Laplace equation in Eq (1.3):

$$P_{\text{max}} = -2\gamma_{lv} \cos(\theta) / r_p \quad (1.3)$$

here θ is the contact angle, γ_{lv} is the pore fluid/ vapor surface tension and r_m is related to the pore radius r_p . The tension developed in the liquid is transferred to the solid gel network, causing it to shrink. Shrinkage is resisted by the bulk modulus of the network K_p which increases with shrinkage or relative density as a power law given in Eq (1.4):

$$K_p = K_o(V_o/V)^m \quad (1.4)$$

where K_o is the bulk modulus of the initial gel, V_o is the initial gel volume, V is the shrunken volume, and m is an exponent which has been found to range between 2.5 and 4. Typically m is 3 for bulk silica gels during isostatic plastic compression, as experienced during drying. Shrinkage stops at the critical point when the maximum capillary tension developed in the pore fluid is balanced by the increase in the network modulus. Continued removal of solvent beyond the critical point normally occurs with no further change in volume: thus it is the extent of shrinkage preceding the critical point that establishes the final pore volume, average pore size, and surface area.



P_c is the capillary tension,

P/P_0 is relative pressure of the pore fluid in the overlying gas,

V_m is the liquid molar volume,

V_o is the initial gel volume,

V is the shrunken volume,

γ_{lv} is the pore fluid/ vapor surface tension,

R_g is the gas constant,

T is temperature,

θ is the contact angle,

r_p is pore radius,

r_m is related to the pore radius r_p ,

K_p bulk modulus of the network of the initial gel,

m is an exponent.

1.2.1.3.1 Supercritical drying

As mentioned in the previous section capillary forces during drying process are responsible for the cracking and shrinking of the gels. The magnitude of the interfacial pressure in the capillary can be calculated as 22.5 atm by equation 1.3, when θ value is taken

0 which is close to the contact angle of ethanol on glass, γ_{lv} is taken 22.39 as $\text{mN}\cdot\text{m}^{-1}$ at 293K and an average pore radius of 20nm is used. This force acts to the small area of the meeting point of the meniscus and the wetted capillary wall. The wall can not stand that much pressure on such a small area and collapses inwards.

This can be avoided by removing the pore liquid above the supercritical conditions where there is no distinct boundary between vapor and liquid phases. There are two ways of supercritical drying each will be explained in different sections; a) High temperature supercritical drying, b) Low temperature supercritical drying.

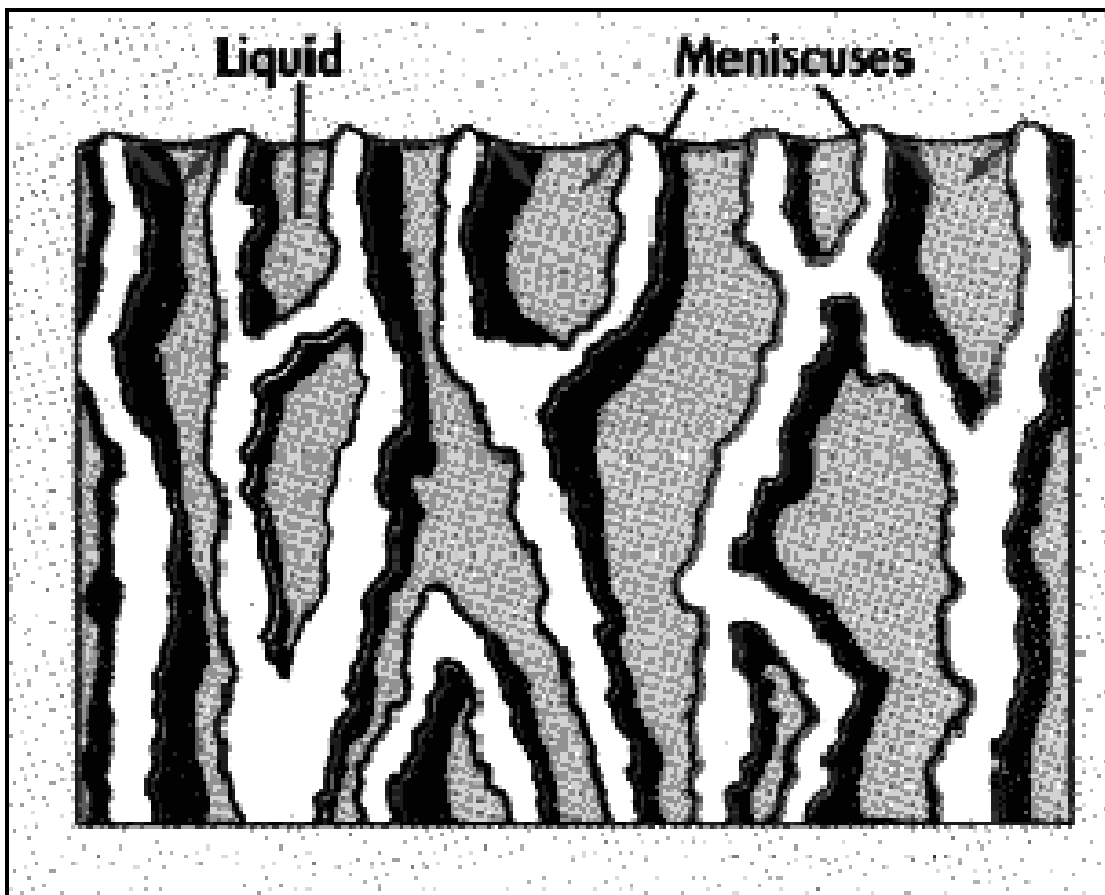


Figure 1.6 Representation of a porous wet gel filled with pore liquid.

High temperature supercritical drying

This process, which was also used by Kistler in 1931, is a very common way to produce silica aerogels. The process starts with placing the wet gel and a sufficient amount of solvent in an autoclave. Temperature is slowly increased which causes an increase in the pressure. After the pressure and temperature are adjusted above the supercritical values of the

solvent, these conditions are kept constant for a certain period of time. Then the vessel is depressurized by venting the liquid at constant temperature until atmospheric pressure is reached. Lastly the system is cooled to room temperature. This procedure is represented in figure 1.7 with methanol as the pore liquid.

The gels dried with this method are hydrophobic and show relatively higher transparencies according to the gels dried by other drying techniques. This is because of the reesterification reactions on the surface of the aerogel at supercritical conditions. However this process has safety problems and is a costly method due to the high critical temperatures and pressures of the pore liquids. In 1984, a terrible accident occurred in Airglass pilot plant in Sweden. The problem with the main gasket of their pressure vessel resulted in a leak of 3000 liters methanol at 533K and 86 bars. Kirkbir et al. studied to lower conditions of the drying process by using different pore liquids but they were not able to lower pressure significantly [22].

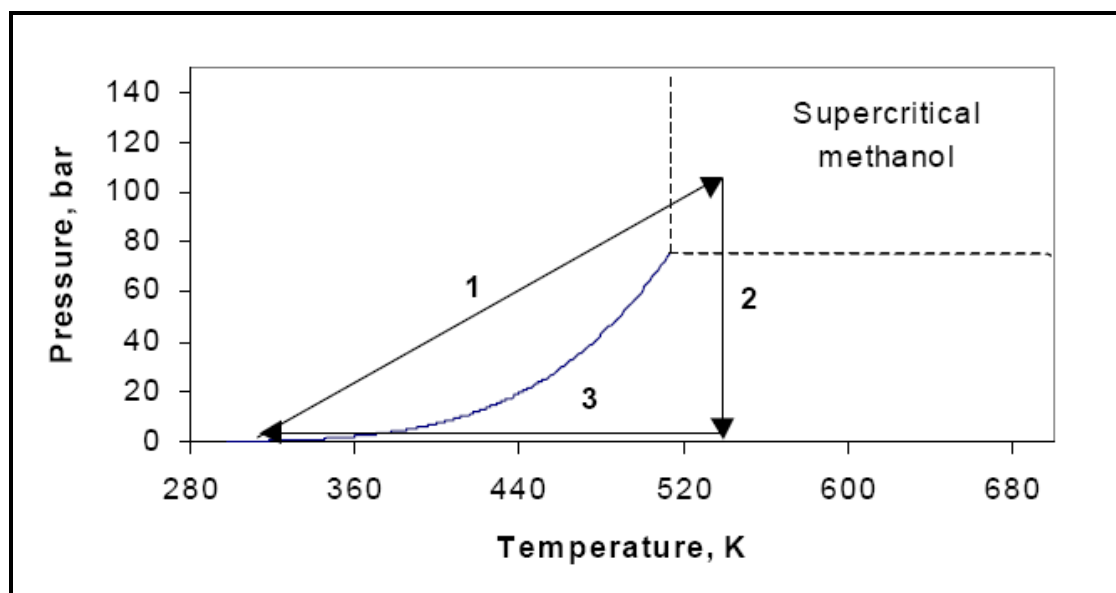


Figure 1.7 High temperature supercritical drying with methanol.

Low temperature supercritical drying

The studies on finding a safer and cheaper alternative drying method gave results in 1985; Tewari et.al suggested exchanging the pore liquid with another one having a lower critical temperature and pressure. Carbon dioxide was found to be the best choice for this purpose among freons being safer and cheaper [23]. The process first applied in 1985 is

represented in figure 1.8 and starts with pumping liquid carbon dioxide into a vessel containing the wet gel and a sufficient amount of alcohol just to cover the wet gel. When the pressure reaches 100 bars, the outlet valve is opened and the extracted solvent with carbon dioxide comes out while keeping the pressure constant. When the effluent becomes alcohol free carbon dioxide, temperature is raised to 313 K through an isobaric path. Then the vessel is depressurized at constant temperature and cooled to room temperature giving hydrophilic aerogels. The extraction process between the first and second steps shown in figure 1.8 is the displacement of the pore liquid with liquid carbon dioxide and is controlled by diffusion which is the most time consuming step of the whole process. The prediction of the process time for complete removal of pore liquid which depends on the type of the pore liquid, diffusion coefficients and thickness of the sample is hard. As the diffusion kinetics of the solvent exchange depend upon the size of the gel, even if a pressure vessel were available to contain a large monolith, the solvent exchange could take weeks to complete, depending on the size of the monolith. If the vessel is depressurized before all the ethanol is extracted from the pores, a non transparent part or even cracks exist in the resulting aerogels.

In 1998 Hajime Tamon et al. studied the effects of extraction temperature, extraction time, depressurizing temperature, and depressurizing rate on the properties of the aerogels [24]. They reported that these conditions do not affect the properties but sol-gel reaction conditions did.

Although supercritical drying with alcohols has the advantages of producing gels with hydrophobicity and higher transparency, the low temperature supercritical drying using CO₂ became a widely used method. This is because of the lower supercritical conditions of carbon dioxide having also the advantages of being non-flammable and chemically inert. The transparency of the CO₂ dried samples can be achieved by a post drying treatment which is simply heating the dried aerogels under atmospheric pressure in air. Tewari et al. further studied the CO₂ drying method to improve the transparency of the aerogels over the alcohol dried ones [25]. After that Tajiri et al. used four supercritical media: methanol, ethanol and isopropanol for high temperature supercritical drying and CO₂ for low temperature supercritical drying. The most transparent aerogel piece was the CO₂ dried one with a solar transmittance of more than 90%, but after treating all the samples at 773K for 2 h, it was the isopropanol dried aerogel which exhibited the highest solar transmittance, nearly 96%, while the CO₂ dried one remained unchanged.

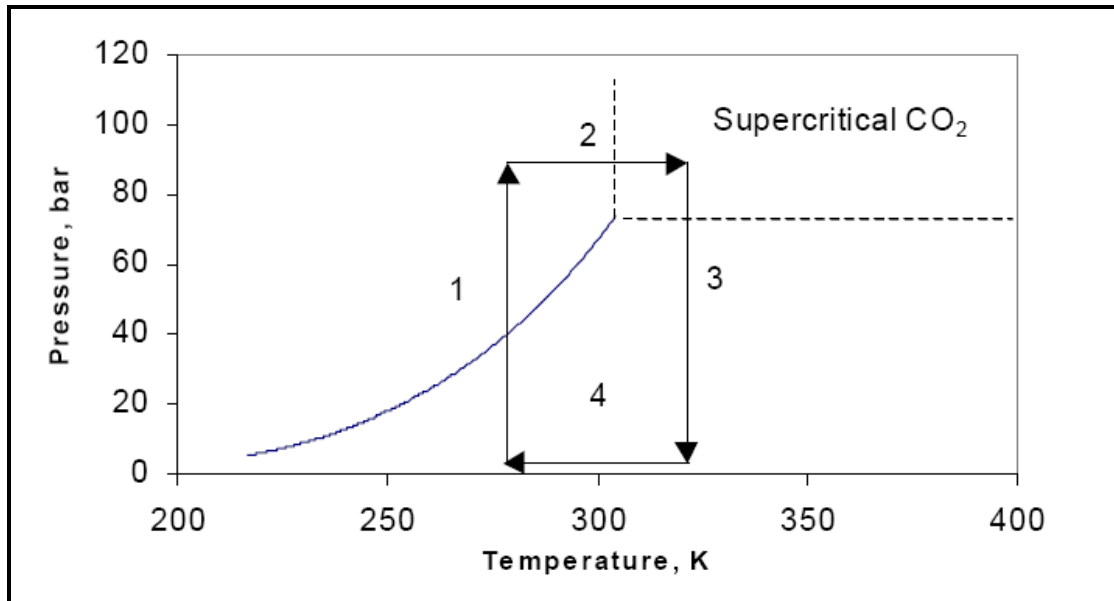


Figure 1.8 Low temperature supercritical drying with carbon dioxide.

1.2.1.3.2 Ambient Pressure Drying

Both low temperature and high temperature supercritical drying methods are expensive due to the operating pressures and required equipment. This is why there is still a great interest in ambient pressure drying. The gels dried by this method are called xerogel. This procedure offers great promise to lower costs for aerogel production which in turn will be very helpful for further development of these materials. Ambient-pressure methods for silica aerogels include both surface modification and network strengthening. Additionally, the contact angle between the pore liquid and the pore walls has to be influenced so as to minimize capillary forces. In general there are two different methods for the surface modification of the gels. First one is the so called co-precursor method in which a surface-modifying agent is added to the silica sol before gelation. The second one is called the surface derivatization method in which after the gel is obtained, it is immersed in a bath of a solvent and a surface modifying agent. The second method was widely used for the synthesis of water glass based silica aerogels via ambient pressure drying method. The disadvantage of this method is that since the mass transfer during silication takes place by diffusion large amounts of solvent, long solvent exchange and surface modification times are required. The co-precursor method has the advantage of rapid surface modification also uniform bulk and surface modification by the addition of the surface modifying agent to the sol.

In 1992 Brinker and Deshpande introduced an ambient pressure drying method based on the so-called spring-back effect which involves chemical modification of the inner surface [26]. First a solvent exchange step is performed to have a water-free solvent in the pores of the gel. Then, reaction with chlorotrimethylsilane takes place so that SiOH groups on the inner and outer surface are silylated by which the surface of the aerogel becomes hydrophobic. After another solvent exchange, drying takes place by evaporation. During drying the silyl-modified gels begin to shrink due to the development of capillary forces. When the liquid phase starts to form isolated droplets within the gel network, since neighboring surface silyl groups are chemically inert and detach with little activation energy, the gel body re-expands. The images of the wet dried and re-expanded gels are represented in figure 1.9.

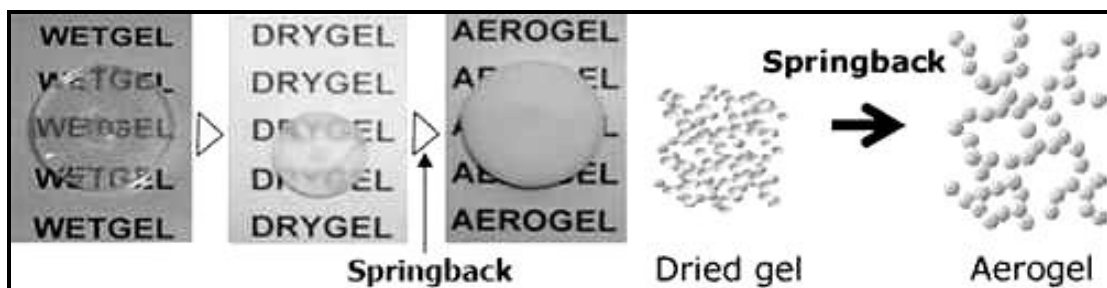


Figure 1.9 Illustration of the spring back effect

Schwertfeger et al. suggested a method for eliminating the solvent exchange step by using water glass as a cheap silica source and employing a silylation agent [27]. The silylation agent also reacts with the pore water in addition to surface modification producing a low tension organic solvent which is suitable for ambient pressure drying. The hydrogel is placed into a solution of hexamethyldisiloxane (HMDSO) and trimethylchlorosilane (TMCS). TMCS reacts with the hydroxyl groups on the gel surface yielding the preferred $-O-Si-R_3$ surface groups, while HCl is released into the water phase. The silylation process is shown in figure 1.10. Furthermore, TMCS reacts with the water at the HMDSO-water interface to form HMDSO and HCl. As HMDSO is poorly miscible with water, phase separation occurs and the aqueous HCl phase is expelled from the pores. Finally, the HMDSO soaked gel is dried at ambient pressure. Such aerogels are normally hydrophobic. Their group has also shown that such aerogels can be turned into hydrophilic materials by oxidation of the surface groups [28]. Rao et al. reported that aerogels retained the hydrophobicity up to a temperature of 325 °C in

air and to 450 C in N₂ atmosphere and lost it above this temperature [29]. This is due to the fact that at this temperature, the Si-CH₃ groups get oxidized into Si-OH, which are responsible for adsorption of water. Recently Rao et al. investigated the properties of ambient pressure dried silica aerogels with waterglass precursor using various silylating agents. The physical properties of the aerogels such as density, porosity, pore volume, thermal conductivity and contact angle measurements were studied by using various mono, di and tri alkyl or aryl silylating agents such as vinyltrimethoxysilane, phenyltrimethoxysilane, phenyltriethoxysilane, dimethyldimethoxysilane, trimethylmethoxysilane, bis(trimethylsilyl)acetamide, methyl trimethoxysilane (MTMS), methyltriethoxysilane (MTES), trimethylchlorosilane TMCS and hexamethyldisilazane (HMDZ). The best quality in terms of low density, high hydrophobicity, low thermal conductivity, high porosity and high optical transmission was obtained with tri alkyl silylating agent such as HMDZ agent [29].

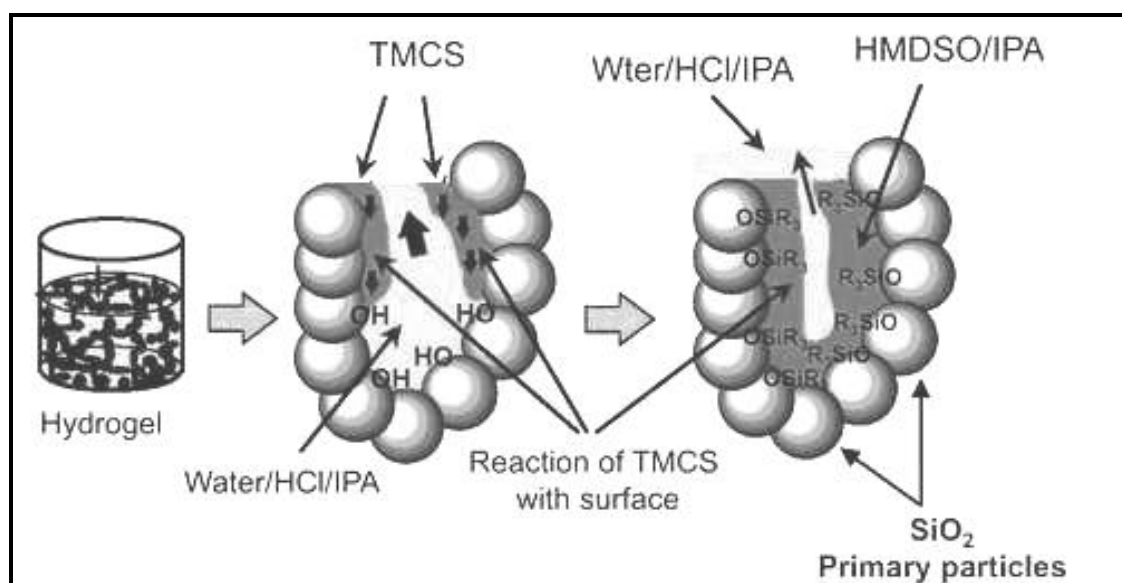


Figure 1.10 Schematic representation of the silylation process.

1.2.1.3.3 Freeze Drying

In freeze drying the idea is that there is no phase boundary between the liquid and gas phase thus the capillary pressure does not play an important role. Here, the solvent must be exchanged with a low expansion coefficient and a high sublimation pressure. The pore liquid is frozen and sublimed under vacuum. Material obtained by this way is called a cryogel.

Unfortunately, freeze drying has many disadvantages including the fact that the aging period has to be prolonged for stabilization of the network and, in some cases; the network may be destroyed by crystallization of the solvent in the pores.

1.2.2 Carbon Black Silica Aerogel Composites for High Temperature Thermal Insulation

It is known that silica aerogels are superior to the existing systems as transparent thermal insulators. However, when it comes to higher temperature applications other than windows, where transparency is not so important, infrared opacified aerogels can be an alternative solution by decreasing the radiative heat transport which can not be neglected at elevated temperatures. The specific infrared extinction of pure silica aerogels for wavelengths m is very low which leads to a significant increase of radiative heat transport with temperature.

There have been a few studies to improve the thermal insulation character of silica aerogels by using carbon as an opacifier. E. Hümmer et al. did some work with carbon soot as filler to the silica aerogels and focused on the improvement of thermal insulation behavior of the powdered composite aerogels [30]. They compared different sized powders of opacified silica aerogels with a monolithic one having the same amount of carbon soot. It was shown that using finer powders of opacified composite aerogels can even be a better solution at vacuum conditions but when at atmospheric pressures, monolithic sample with carbon soot shows the lowest thermal conductivity. In opacified monolithic samples with different carbon sources, the radiation was effectively blocked. However, in order for the granular or powder samples to have the same insulation performance as monolithic ones, vacuum has to be applied to the powdered systems (figure 1.11).

M. Smith and his coworkers modified the surface of carbon black before adding it to the silica sol and checked the effect of this process on the thermal performance of the granulate compacts [31]. They again concluded that the particle size is important in controlling the efficiency of insulation. However, as the particle size decreased under $100\text{ }\mu\text{m}$, it got harder to handle the aerogel powder. They also synthesized 2 types of monolithic aerogels; one with carbon black and the other with surface modified carbon black which is dispersed in water before addition to the sol. The modified carbon black showed lower thermal conductivities which was attributed to better dispersion of the carbon black powder in

the silica matrix. Among these results this paper does not include pore characterization of these composite aerogels.

Similar to the efforts to improve the thermal insulation performance of the silica aerogels at high temperatures, composite aerogels were investigated as a solution to improve their mechanical properties. K. E. Parmenter and his coworkers added a fiber mixture consisting of silica, aluminaborosilicate and alumina into the silica sol after the hydrolysis step to check the effects on mechanical properties of the composite monoliths [32]. It was concluded that the amount of fiber reinforcement did not affect the hardness and compression strengths of samples in a noticeable way but it caused an increase in the secant moduli of the samples with an increase in the fiber reinforcement percentage. They related these effects to the density changes of the samples having different shrinkages. In 2001, Moner-Girona et al. reported on mechanical behavior of monolithic silica aerogels produced by sol-gel technique with different amounts of activated carbon added just before gelation [33]. This study showed that addition of small amounts of carbon (0.02 - 0.5 wt%) resulted in an increase in the elasticity of the samples with nearly same hardness values. They gave a possible explanation of the increase in elasticity as the carbon disturbs the cross-linking of the silica matrix resulting in a less rigid structure. These studies showed that carbon addition to the silica aerogel is a promising way to improve insulation and mechanical properties.

In the studies mentioned above on carbon-silica composite aerogels [30-31-32-33], the effects of carbon addition and carbon content on the pore properties and the micro structure of silica aerogels were not investigated. Such data are necessary in development of models for predicting thermal conductivity in porous composite materials and for determination of optimum carbon content for minimizing thermal conductivities. The data on the micro structure is beneficial to determine the extent of mixing of the two materials at the micro scale and to improve the dispersion of the phases.

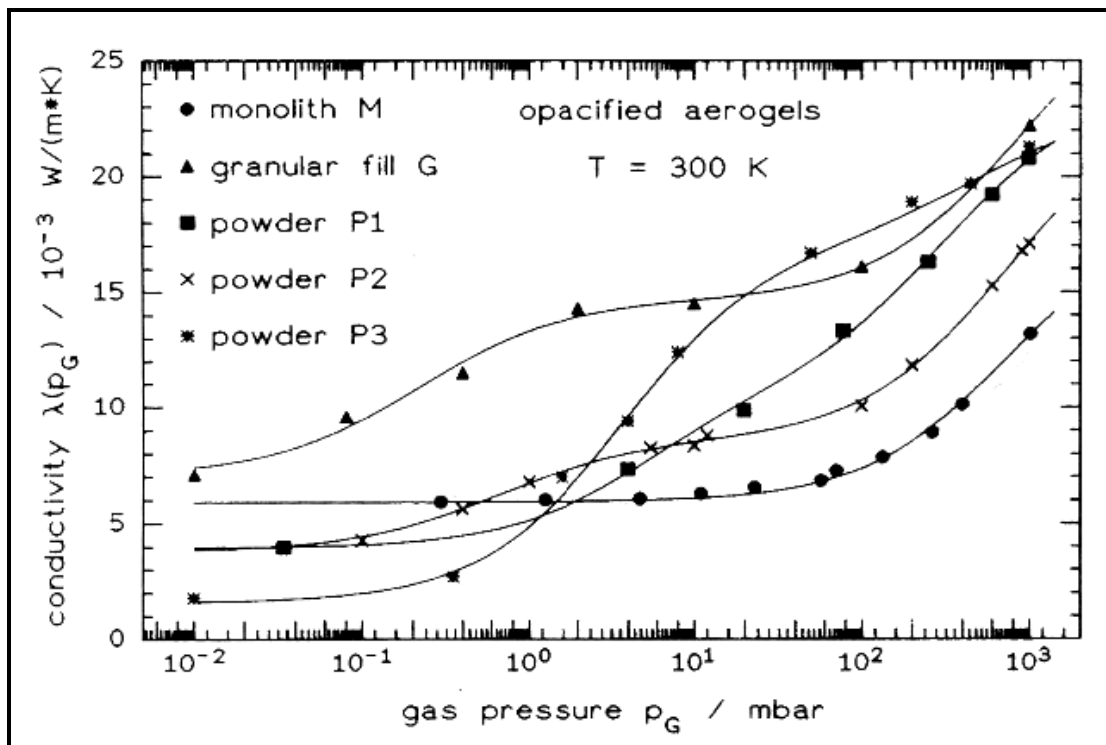


Figure 1.11 Variation of thermal conductivity of different opacified aerogel insulants at 300 K with air pressure [30].

Radiative Heat Transfer

Radiation is the energy streaming through space at speed of light. All substances with a temperature greater than absolute temperature emit radiation that is called thermal radiation. This radiation can be reflected, absorbed or transmitted but is eventually absorbed after many reflections and once absorbed it is no longer radiation and is converted to heat. Net energy is the difference between energy emitted - energy absorbed while conduction and convection independently takes place. Combined heat transfer by convection and radiation can be written as [34]:

$$\frac{q_c}{A} = \frac{q_c}{A} + \frac{q_r}{A} = (h_c + h_r)(T_1 - T_2) \quad (1.5)$$

where q_c is the heat transfer rate by convection and q_r is the heat transfer rate by radiation. T_1 is the temperature of surface and T_2 is the temperature of air and the enclosure. h_r can be expressed as [34],

$$h_r = \frac{\varepsilon \sigma (T_1^4 - T_2^4)}{T_1 - T_2} \quad (1.6)$$

where, ε is the emissivity and σ is a constant ($5.676 \times 10^{-8} \text{ W/m}^2 \cdot \text{K}^4$).

It is difficult to predict the radiative heat transfer in porous media. When the structure of the medium is well defined, it is possible to model the radiative transfer and provide detailed radiative transfer information using the characteristics of both the physical structure and surface radiative properties of the porous material. However for this model, a lot of information such as the directional and spectral emissivity and reflectivity of the structural elements and their detailed geometry are required which are usually not available. Moreover when the elements of the structure are not opaque, then the problem becomes more and more complicated since refraction at the solid fluid interface of the elements and the external and internal reflections that occur at these interfaces should be considered. An even more difficult problem arises if the elements of the porous medium are so closely spaced that reflected radiation from one element is affected by the reflected radiation from adjacent elements. These effects cause the subject to be considered with dependent scattering making the analysis and correlations very difficult. Singh and Kaviany concluded that independent theory is shown to fail for systems with low porosity and is not suitable for packed beds ... and noted that deviations from independent scattering theory are significant for porosities as high as 0.35 [35]. They point out that when temperature gradients are large and/ or the thermal conductivity of the elements is small, the assumption of isothermal elements may fail, and the analysis of radiative transfer among elements must account for this fact [35].

Wang et al. studied prediction of the effective thermal conductivity of high-porosity open-cell porous foam materials by using models [36]. Also experiments were performed for comparison to the model results. Effective thermal conductivities of reticulated vitreous carbon (RVC) foams with water or air as the fluid media were predicted and compared with the existing experimental data. The RVC water predictions agreed well with the experimental data while the RVC-air predictions were a little lower than the experimental results. They thought that the effects of thermal radiation may become more significant when the overall effective thermal conductivity of media is relatively low. To verify their speculation, they added the thermal radiation contribution to their calculation using the existing models for radiative heat transfer. The simple relationship between the radiation contribution k_{rd} to the thermal conductivity and the temperature T for polyurethane (PU) foams in literature can be written as:

$$k_{rd} = \frac{16\sigma T^3}{3(42.038\rho_{\square\square} + 121.55)} \quad (1.7)$$

where σ is the Stefan-Boltzmann constant ($5.67 \times 10^{-8} \text{ W/m}^2 \text{ K}^4$), T is the mean temperature, ρ_s is the solid density and V_s is the solid volume fraction. Figure 1.12 shows the predictions of effective thermal conductivities of PU foams at 286K with and without the radiation modification, in comparison with experimental data. After the radiation modification the effective thermal conductivities agree pretty well with the experimental data for PU foams under both a standard air pressure and a low air pressure. The results also show that the importance of radiation contribution decreases with an increasing solid volume fraction so that the two simulation results converge at high solid volume fraction; e.g., the radiation contribution accounts for almost 6% when the solid volume fraction is over 10% for 286 K and standard air pressure conditions, as indicated in figure 1.12.

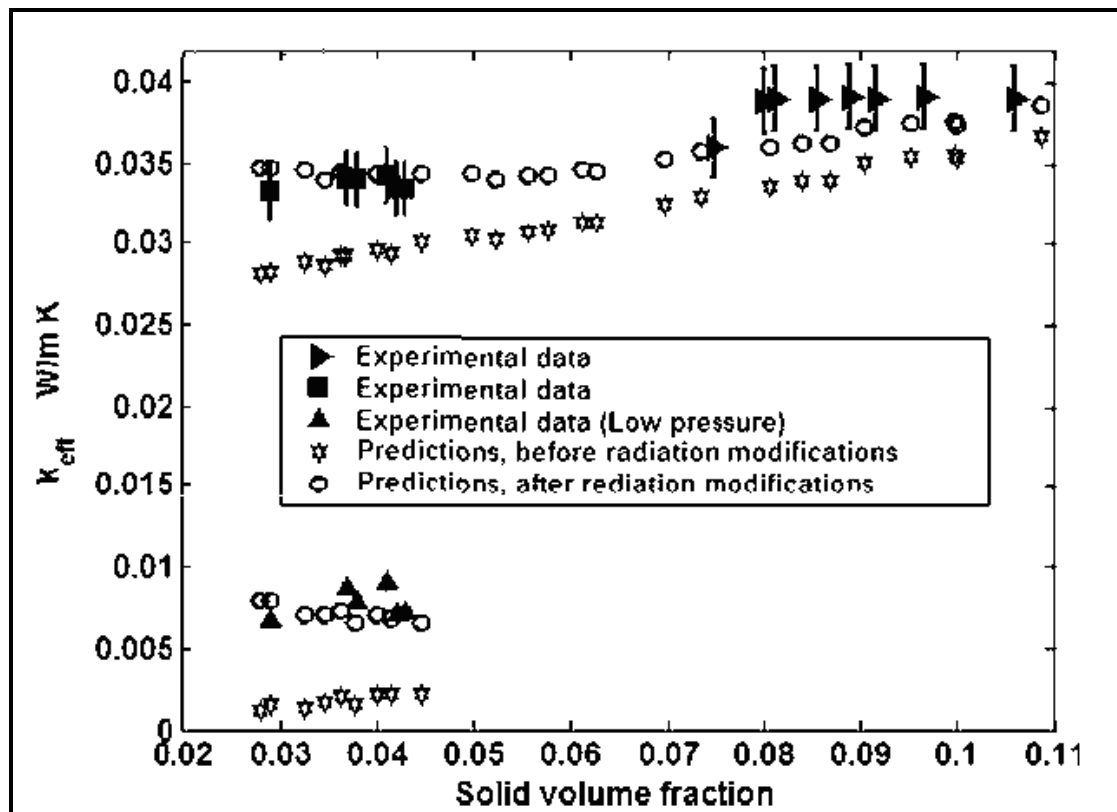


Figure. 1.12 Comparisons of effective thermal conductivities of polyurethane foam samples against the solid volume fraction in polyurethane foams [36].

In 2005, Reim et al. investigated several properties of granulate silica aerogels for development of glazing windows [37]. In this study they also measured the packed beds of silica aerogel granulates thermal conductivity depending on temperature, with a gas pressure

of $P_{\text{gas}} = 1$ mbar and under an external load of $P_{\text{ex}} = 3.2$ bars. They reported that the temperature dependence of the thermal conductivity is mainly caused by radiative transfer, which can considerably exceed the heat transport via solid and gas, since the radiative thermal conductivity λ_{rad} increases by the third power of the absolute temperature T for radiative diffusion:

$$\lambda_{\text{rad}} = \frac{16}{3} \frac{\sigma \cdot n^2}{e^*(T) \rho} T^3 \quad (1.8)$$

Here, n is the effective refraction index of the material with the density ρ and σ is the Stefan Boltzmann constant. The mass specific extinction $e^*(T)$ is a temperature-dependent material value characterizing the radiative attenuation, which should be as large as possible for effective insulation. Figure 1.13 shows the results of this study and how thermal conductivity increases at high temperatures.

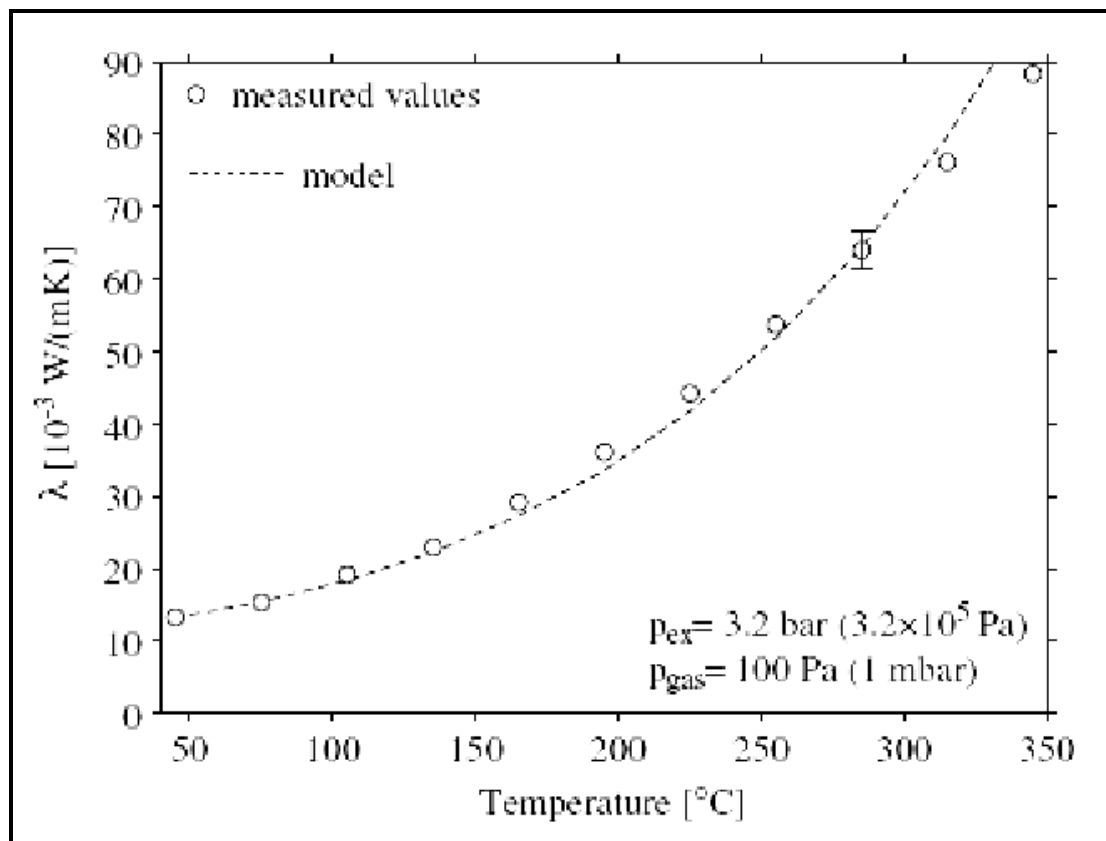


Figure 1.13 Measured and calculated total thermal conductivity depending on the temperature at 3.2 bar ($3.2 \cdot 10^5$ Pa) external load and a gas pressure of 100 Pa (1 mbar) [37].

In 1992 Hümmer et al. used carbon soot to develop granular aerogels that are effectively IR opacified [30]. They considered the thermal transport in opacified aerogel monoliths as an additive superposition of solid, gaseous and radiative conductivity. The solid conductivity, λ_s , strongly depends on the density and the temperature dependence is comparable with the vitreous silica. The gaseous conductivity, λ_g , is much smaller than the conductivity of non-convecting air (0.026 W/m K at 300K) which is the result of the largest pore size of the aerogel is comparable with the mean free path of the air molecules at 1 bar. The radiative conductivity, λ_r , in opacified aerogel monoliths depends on temperature and IR-extinction coefficient, $E = \kappa \rho$. The specific extinction, κ , can be determined calorimetrically or by IR-optical measurements. Typical values for opacified aerogels are 30-60 m²/kg. Using these correlations they calculated the effective thermal conductivities of opacified monolithic aerogels depending on their densities at different temperatures. The significant effect of radiation with increasing temperature can be observed in figure 1.14.

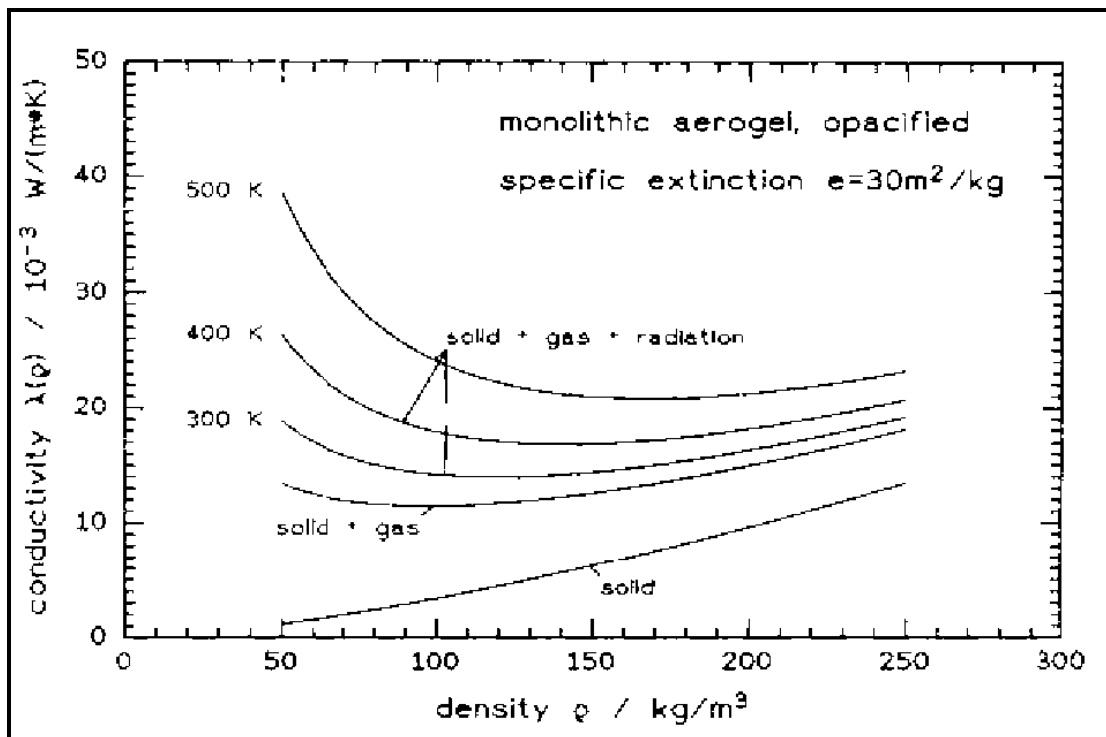


Figure 1.14 Calculated variation of thermal conductivity of opacified aerogels as a function of density, for temperatures 300, 400 and 500K [32].

1.3 Objectives:

The first part of the study aims to gain knowledge on preparation of monolithic and transparent aerogels with low thermal conductivities. There is a huge literature on preparation of these novel materials with many different methods. We first decided to obtain this background with literature and improved our experience with hands on experiments. Although this study does not include optical or thermal characterization, these properties were tried to be optimized by the correlations given in literature. Decreasing pore sizes and increasing porosity serves for the improvement of both of these physical properties to be a better transparent thermal insulation material.

The main purpose of this study is to prepare carbon black – silica composite aerogel materials with different carbon contents and report the effects of carbon content on the pore properties and the micro structure of silica aerogels which were not investigated in literature. It will help to develop models for carbon – silica composite aerogels for predicting thermal conductivity in porous composite materials.

Carbon – silica composite aerogels were chosen to be studied because this is a very promising way to obtain very effective thermal insulation solutions at high temperatures. Since the thermal insulation performance of aerogels is very dependent on pore properties of these materials this will be a very useful data for future studies on carbon-silica aerogel composites.

Chapter 2

EXPERIMENTAL

2.1 Synthesis

The two step sol-gel method was chosen to be able to use the advantage of the ability to combine both acid and base hydrolysis to control the microstructure of the aerogels. Also in case of very dilute solutions, performing the hydrolysis reaction in an acidic media lowers the gelation time from hours or even days to minutes.

Silica aerogels in this thesis were synthesized using TEOS (FLUKA purun: > 98.0 % (GC) as the precursor, HCl as the hydrolysis catalyst and NH₄OH (ALDRICH 2.0M in ethanol) as the condensation catalyst. TEOS was diluted with ethanol at different concentrations (20/30/40/50/60/70 wt%). Subsequently, water and acid catalyst were added to start hydrolysis under continuous stirring. Condensation started with the addition of the base catalyst and the sol was taken into syringe molds (5ml cylindrical) for complete gelation. The overall ratio of TEOS: Water: HCl: NH₄OH was kept constant as 1: 4: 0.00244: 0.02. The complete process is summarized in figure 2.1 and the reader can find the details of these steps in the following sections.

2.1.1 Synthesis Solutions

The sols were prepared as the masses of TEOS and ethanol add up to 5g. The reactants were weighed on an analytical balance in a 10ml beaker. For example, 20 wt%, TEOS corresponds to a mass ratio of TEOS/Ethanol = 0.25. The amount of catalysts and water to be added were calculated from the mole ratios of these materials and TEOS which is TEOS: Water: HCl: NH₄OH; 1: 4: 2.44×10^{-3} : 2×10^{-2} . The detailed synthesis solutions are given in table 2.1.

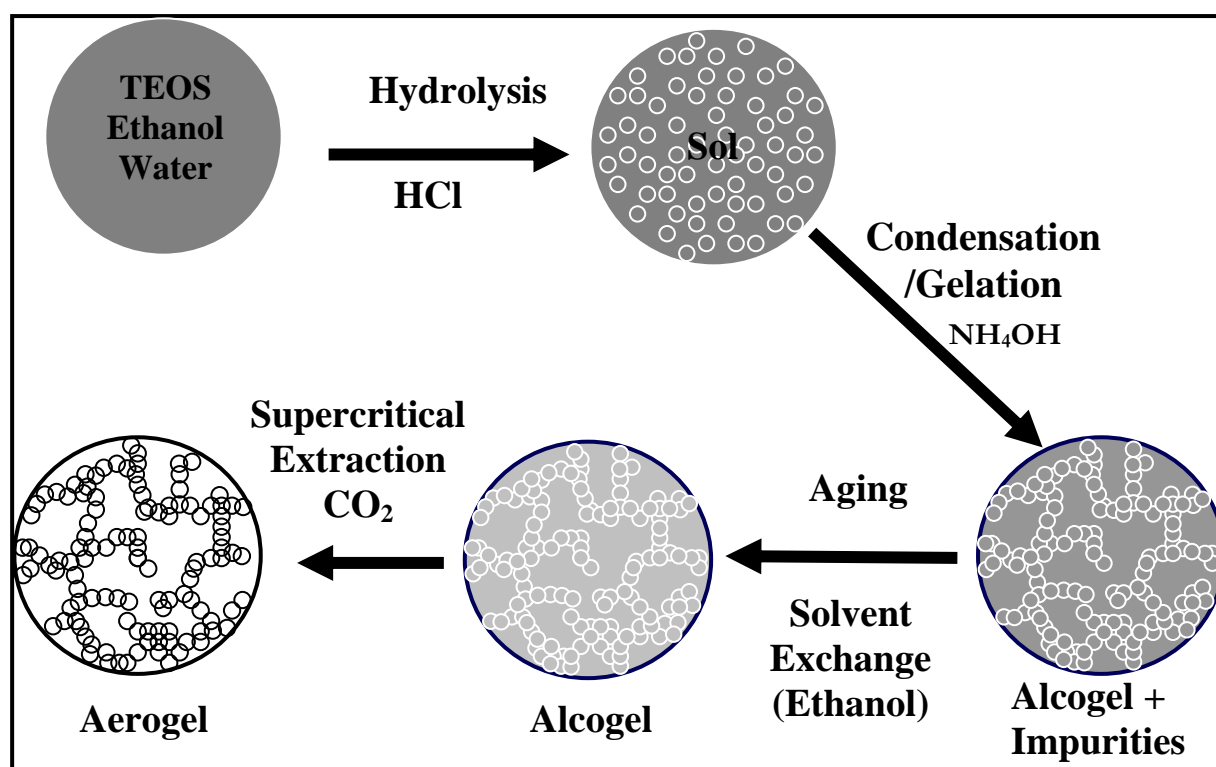


Figure 2.1 The schematic representation of the procedure during silica aerogel synthesis by sol-gel method.

Table 2.1 Reactant amounts for one sample preparation.

TEOS wt %	TEOS (g)	ETHANOL (g)	WATER (g)	4.89×10^{-2} M HCl (ml)	0.4M NH_4OH (ml)
20	1	4	0.35	0.2	0.4
30	1.5	3.5	0.52	0.31	0.6
40	2	3	0.70	0.4	0.8
50	2.5	2.5	0.85	0.5	1
60	3	2	1.03	0.62	1.2
70	3.5	1.5	1.21	0.7	1.4

After water is added, acid catalyst is put into a beaker and the beaker is covered with a stretch film. The solution is stirred in the beaker on a magnetic stirrer for 40 min. Desired amount of base catalyst is then added drop by drop into the sol under continues stirring. The sol is immediately taken into a mold before gelation starts. The gelation time changes with changing TEOS concentration in the sol. This time can be as low as a few minutes which start

with the addition of the base catalyst and some times there was not enough time to take the sol into the mold. This problem was solved by optimizing the base catalyst concentration and addition rate by performing several experiments with different concentrations and addition rates. Also at high TEOS concentrations, it is better to have a mold that can be loaded and sealed fast.

Gelation is observed by shaking the mold and observing the increasing viscosity. The gels were smashed when we tried to get out them just after gelation point is observed. The network formed at gelation point is strong enough to avoid the liquid part of the gel from flowing away, but it is not that strong enough for removal from the mold. This problem was solved by aging the samples in the molds for 1 hr after the gelation point was reached. One has to be fast while taking the gel out of the mold and transferring it into a solution. The duration is critical to avoid evaporation of the pore liquid and to avoid crack formation.

Another critical issue is to take the gel out of the mold as a monolith. At first, a glass test tube was used as a mold and the mouth of the test tube was closed by a stopper. It was not possible to take the gel out of the test tube after the gelation point was reached because the gel was stuck in the test tube. When the tube was broken in order to get the gel out, the gel was broken too. Another way was to fill the tube with the sol and seal the mouth with the stopper then to turn the tube upside down before gelation. After the gelation point and 1 hour aging in the tube, the bottom of the test tube was broken and the stopper at the mouth was removed. Then the gel was like in a glass tube open from both ends. It was possible to push the gel from one side and to take it out from other side but the gel was broken while removing the stopper. It was observed that the wet gels can be taken out by pushing them; this gave the idea to use a syringe as a mold. The 5 ml syringes were chosen when the vessel dimensions, which is used in the drying step, were taken into consideration. The diameter of a 5ml syringe is 1.23 cm. The sol could be easily taken into the syringe and was sealed easily. After gelation, the syringe was cut from the sealed part and easily pushed into the aging solution. By this way we were able to produce cylindrical crack free monoliths.

The next molding study was to produce a flat shaped monolith. The gels did not stick to Teflon as they stick to glass. A ring shaped Teflon mold system was custom manufactured. A glass plate was put at the bottom of the Teflon ring, and a metal plate was put at the top of the ring. The ring was sandwiched between the glass and the metal plate which were than

compressed with the help of 4 screws. The sol was injected into the ring from a small hole on the metal plate.

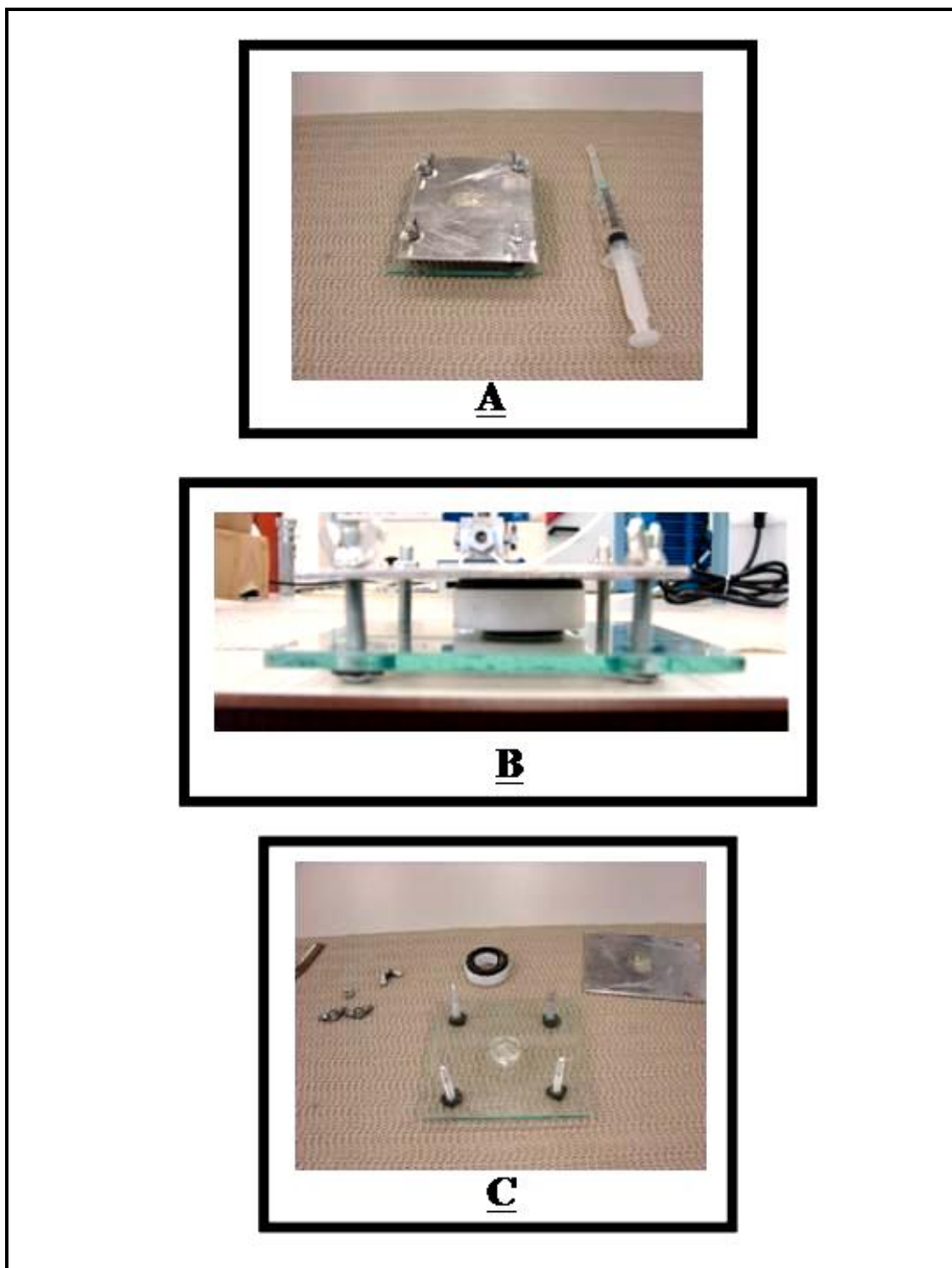


Figure 2.2 The pictures of the two molding systems used in this study. A: Teflon ring mold system and the syringe mold both loaded with sol solutions. B: Front view of the Teflon ring mold that is filled with 2ml sol solution. C: Opened flat mold with the gel on the glass plate.

After gelation finished, the metal plate was removed then the Teflon ring was removed carefully while some ethanol was poured onto the gel in order to avoid evaporation. The gel on the glass plate was taken by the help of a spatula and put into an aging solution.



Figure 2.3 The pictures of two monolithic samples prepared from a flat mold and a cylindrical mold.

Both the Teflon sandwich mold system and the syringe mold are shown in figure 2.2. A shows a closed Teflon sandwich mold system where the small hole can be observed on the metal plate. B shows the front view of the mold where the screws can be observed more easily. C shows the removed metal plate and Teflon ring leaving the gel on the glass plate. Figure 2.3 shows a picture of two samples one of them is monolithic crack free flat sample prepared by the Teflon mold described above. The second one is a cylindrical monolith prepared in a 5ml syringe mold.

2.2 Aging Solutions and Temperatures

Water/Ethanol and TEOS/Ethanol mixtures were used as the aging solutions. The gels prepared from the same sol having a concentration of 60 wt% TEOS were placed in different aging solutions at the same time while the control sample was directly transferred into ethanol. The cylindrical gels were immersed into vials containing the aging solutions, directly from the syringe molds. Water:ethanol and TEOS:ethanol volumetric ratios were 1. Some aging experiments were performed at different temperatures to investigate the effect of temperature on aging. Some of the samples were aged at room temperature; some of them were aged in an oven at 323K in a closed container (vial) to avoid evaporation of the aging solution. The sample that was aged at 373K was aged in a high pressure vessel which was placed in the oven. After 20h in aging solutions at different temperatures, the samples were put in pure ethanol solutions at room temperature in order to get rid of the impurities other than ethanol in the pores of the gels. The gels stayed in ethanol for 4 days before drying.

2.3 Drying Apparatus and Conditions

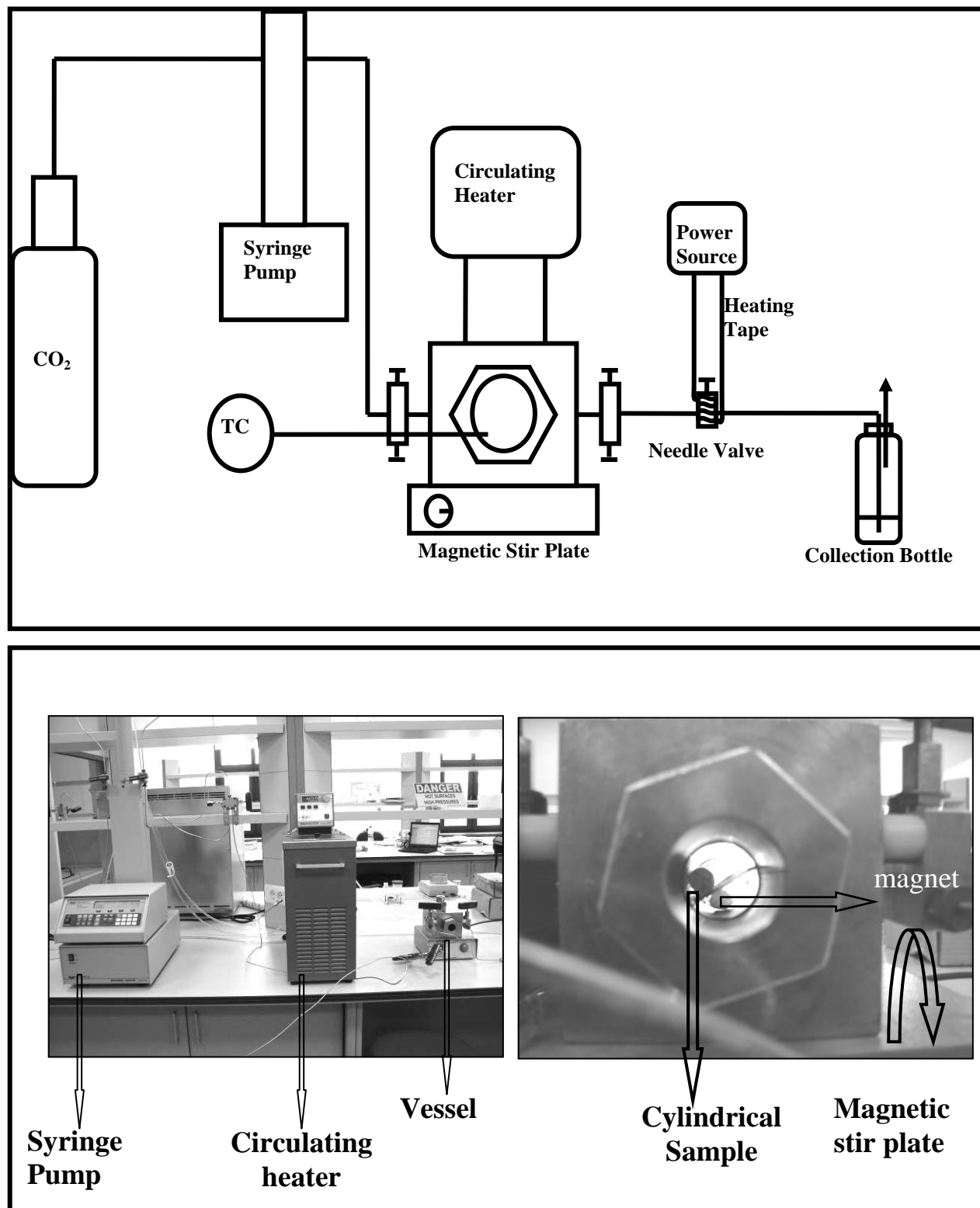


Figure 2.4 A) Schematic representation of the supercritical extraction set-up. B) The image of the experimental apparatus for supercritical extraction.

Ethanol was extracted from the alcogels with supercritical carbon dioxide using the apparatus shown in figure 2.4. A high pressure vessel (custom manufactured from 316 stainless steel) was used which has an internal volume of 54 cc. The vessel is equipped with two sapphire windows (thickness 12mm) for continuous observation. The contents of the vessel were stirred using a magnetic stir bar. A stainless steel screen was placed in the middle of the vessel to separate the stir bar and the monolithic samples.

The temperature of the vessel was controlled with a circulating heater-cooler (Cole Parmer Polystat Temperature Controller Model 12108-15) with the help of the internally machined channels in the vessel. All the procedure was performed at 313K.

An adequate amount of ethanol which is enough to cover the wet gel to avoid evaporation was put in the vessel first. After the gels and the stir bar were placed, the vessel was closed. CO₂ was pumped into the vessel with a syringe pump (ISCO model 260D) until the pressure reached to 82.74 bars, and then extraction was started at constant pressure. This extraction process was performed for 3 days. Since the pump is not a continuous one, the extraction process was not performed continuously for 3 days. Sometimes the temperature of the vessel can become higher than 313K because of the magnetic stirrer and an ethanol layer appears at the bottom of the vessel. It is important to remove all the ethanol initially added before the diffusion process which will take place all night. Since the outlet of the vessel is in the middle of the side wall of the vessel, it was hard to get rid of that ethanol layer at the bottom. Therefore, the pressure was increased until the densities of the two layers became equal and the ethanol layer disappeared. After all the bulk of ethanol is removed from the vessel, the pressure was decreased to 82.74 bars again. After that, the speed of the drying process is mainly controlled by diffusion of ethanol from the pores. It is not necessary to continue to pass carbon dioxide through the vessel during the night. The vessel was generally isolated by closing both inlet and outlet valves in order for removal of the ethanol in the pores by diffusion overnight. The vessel was kept at 313K so that in case of any leak during night, carbon dioxide in the pores of the gel will still be at supercritical conditions. The flow rate was controlled by a heated needle valve. It is better to adjust the flow rate a little high at first until the ethanol placed in the vessel is removed. Since the gels are very brittle, it is better to avoid very high flow rates. We tried not to exceed 200 ml/hr. The second day, it is not necessary to have a high flow rate since diffusion controls the drying time. After the ethanol

present in the pores of the gel was totally replaced with supercritical carbon dioxide, the CO₂ inlet was closed and the vessel was depressurized slowly from the heated needle valve.

2.4 Preparation of Carbon black Silica Aerogel Composite Materials

Cabot Vulcan XC72R was used for the synthesis of carbon black - silica aerogel composites. It is a powdered carbon black having a typical bulk density of 0,096 g/cc. The desired amount of carbon black was added to ethanol and the mixture was stirred for one hour. The amounts of carbon black powder and the resulting composite aerogels are given in Table 2.2. After addition of NH₄OH, the sol was added to the carbon black ethanol mixture. The resulting mixture was stirred for about 5 more minutes and the mixture was taken into syringe molds as shown in figure 2.5. The composite gels were aged in 50% water ethanol solution at 323K for 20h. Then solvent exchange was conducted in ethanol for 4 days before supercritical CO₂ extraction. The carbon weight percentage of the composite was varied from 0.34 % to 4.5 %).

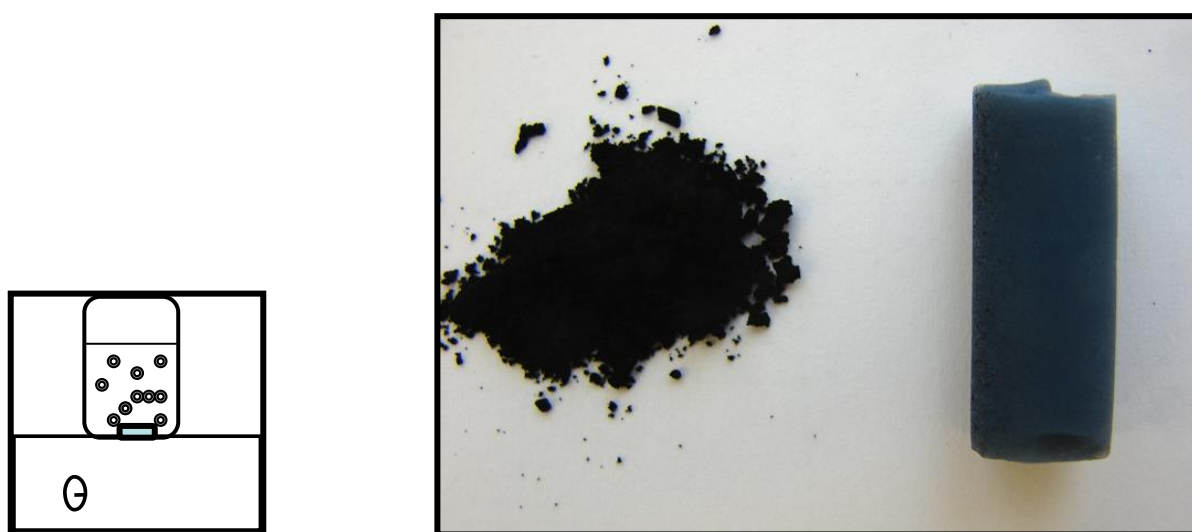


Figure 2.5 Preparation of carbon black silica aerogel composite in a beaker on a magnetic stirrer and carbon black powder and a monolithic composite sample.

Table 2.2 The carbon black amounts used in the synthesis of composite aerogels

Carbon black (wt %)	0.34	1.08	2.29	4.5
Aerogel mass (g)	0.275	0.440	0.273	0.272
Carbon black mass (g)	0.001	0.005	0.006	0.012

2.5 Characterization Methods

2.5.1 Density

There are two density terms to characterize the density of aerogels; a) bulk density and b) skeletal density. Bulk density is simply found by dividing the aerogel's mass to its volume. The volume of the gels in this thesis is calculated by synthesizing monolithic and cylindrical shaped aerogels and measuring their dimensions using a caliper. The mass of the aerogels was determined using an analytical balance.

The solid parts of the aerogels are made up of ultra fine particles whose density is said to be the skeletal density. This value was calculated using helium pycnometry as 2.2 g/cc for silica gels [17].

The porosity and pore volume of the gels can be calculated using these two density values as follows;

$$\% \text{ Porosity} = (1 - \rho_b / \rho_s) \times 100 \quad (2.1)$$

$$\text{Pore Volume} = (1 / \rho_b - 1 / \rho_s) \quad (2.2)$$

here, ρ_s is the skeletal and ρ_b is the bulk density of the aerogels.

2.5.2 Thermo Gravimetric Analysis (TGA)

The thermo gravimetric analysis of the samples was performed to observe the thermal stability of the samples and the extent of water uptake. The analysis was performed using a TG/DTA instrument. The samples were crushed and put in a 20K alumina crucible. The temperature was changed from 298K to 1323K with a heating rate of 20⁰ C/min in an atmosphere of air.

2.5.3 Nitrogen Adsorption/Physisorption Analysis

According to the classification recommended by IUPAC, pores that have diameters less than 2nm are called "micropores"; those have diameters between 2 and 50 nm are called "mesopores", and those have diameters greater than 50 nm are called "macropores". Silica aerogels possess pores of all three sizes but the majority of the pores fall in the mesopore regime, with relatively few micropores. In this study the pore size distribution and pore volume analysis of the gels were performed using Nitrogen Adsorption/Physisorption Instrument (Mettomertics ASAP 2030). The surface area was calculated using the BET

method and pore volume and sizes were calculated using BJH method. In this section brief information will be presented about these methods.

There are many available experimental methods for characterization of porous materials including gas adsorption, mercury porosimetry, electron microscopy, thermoporometry, NMR-methods and others. Each one has a limit on pore size analysis in terms of length scale which was given by IUPAC. Among them gas adsorption is the most popular one suitable for determining a wide range from 0.35nm to 100nm. In addition that it is convenient to use also it is not that costly when compared to some of the other methods. The pore characterization of aerogels is difficult because of the capillary pressures applied by conventional methods. Since silica aerogels have high porosity and small pore sizes this cause large volumetric compressions which lead to incorrect pore size and volume determination [12]. The most widely used method for determination of aerogel porosity is the nitrogen adsorption/physisorption technique. In this method surface area and pore size analysis is usually based on nitrogen, argon and krypton adsorption isotherms obtained with the volumetric method at temperatures of liquid nitrogen (77.35K) and liquid argon (87.27K). The shape of these isotherms depends on pore size and temperature of the porous material [38].

□□□□□□□□□□□□□□□□

Adsorption is the process of a selective transfer of a fluid phase to the surface of an insoluble solid. The adsorption caused by Van Der Waals forces is called physical adsorption, physisorption. The interaction energy of a gas molecule at a distance z from the solid surface is approximately given in Eq(2.3) [38]:

$$C_{sf}(z) = \frac{\pi C_{sf} \rho_s}{6 z^3} \quad (2.3)$$

where C_{sf} is a measure for the strength of attractive fluid- solid interactions and ρ_s is the solid density. At temperatures below the boiling point of the adsorptive, the system can be treated as an adsorbed phase coexisting with the bulk phase which is the situation with nitrogen at temperatures of liquid nitrogen [38]. Physisorption is reversible, except in some cases of multilayer adsorption such as filling in capillary pores where hysteresis occurs. The physisorbed density is not in the order of magnitude of the liquid or the vapour state.

□

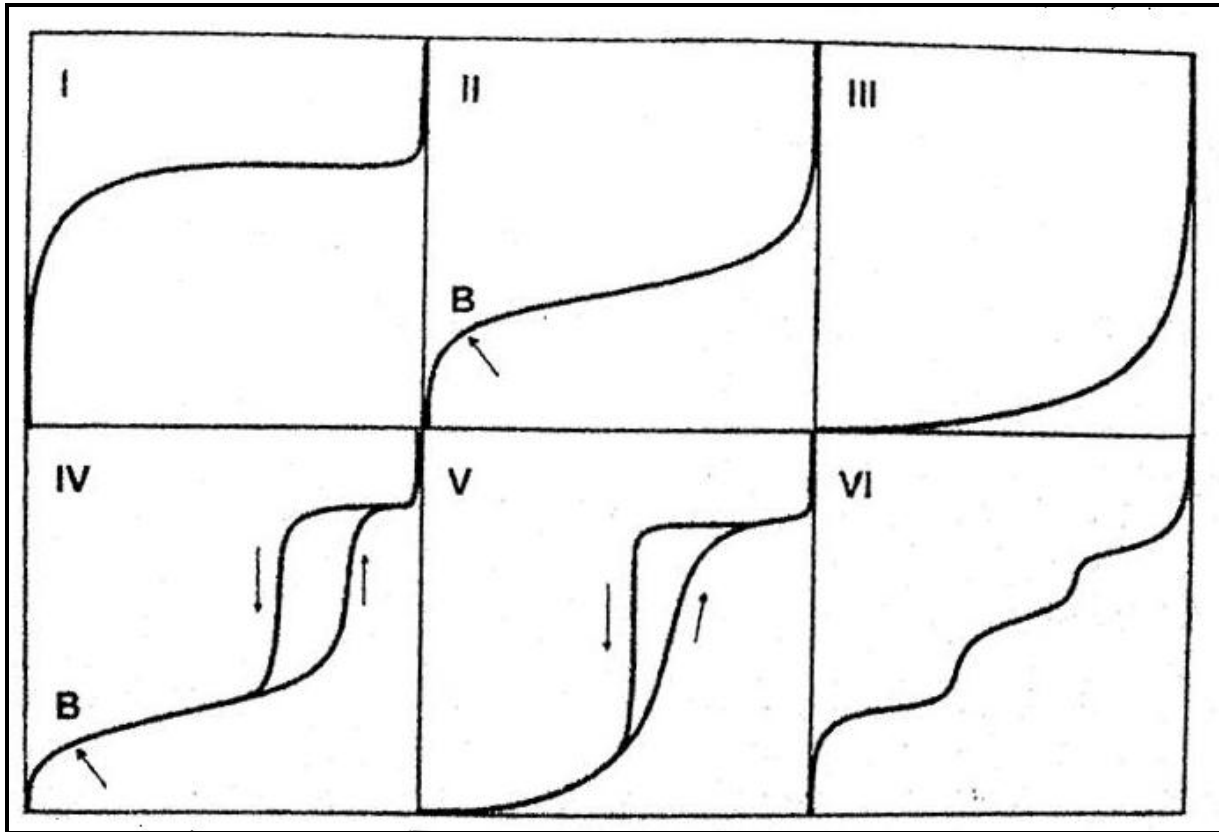
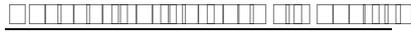


Figure 2.6 The six types of adsorption isotherms classified by IUPAC [38].

A plot of adsorption amount n , as a function of pressure P , at constant temperature T , is the adsorption isotherm of a gas or vapor system. In literature a database of tens of thousands of isotherms were collected and many of these isotherms fit into one of the six isotherms which are published by IUPAC [38]. Figure 2.6 shows these 6 types of isotherms which can give information on the surface and pore characteristics of the adsorbent. Type I is typical for materials having micropores and small external surfaces such as molecular sieve zeolites, activated carbons where adsorption is limited to at most a few molecular layers. Type II isotherms are typical for non-porous or macroporous materials showing unrestricted monolayer-multilayer adsorption. Type III is seen when the interaction of adsorbate and adsorbent is weak which is relatively not common. Type IV and V isotherms exhibit hysteresis loops which are the result of capillary condensation in the mesopores. Type IV follows the same path as Type II initially which is obtained from a nonporous form of the adsorbent. Type V is not common as Type III where adsorbent-adsorbate interaction is weak.

The last type is a new rare type recently identified. Type VI shows the stepwise multilayer adsorption on a uniform non-porous surface [39].



The description of different adsorption isotherms are done with some mathematical models including the Langmuir Model, the Freundlich Model and the Brunauer, Emmett and Teller Model (BET). The BET theory is the extended version of the Langmuir adsorption model to be applied to multilayer adsorption. According to BET theory, once a layer is adsorbed to the surface it becomes another adsorption site for the next layer.

The BET theory is based on several assumptions:

- 1) adsorbent consists of a regular array of adsorption sites equal in energy, with a constant enthalpy of adsorption in the monolayer
- 2) adsorption is localised to these sites
- 3) neighbouring adsorbed molecules do not interact
- 4) multilayer formation is unlimited
- 5) enthalpy of adsorption in second and subsequent multilayers is equal to the enthalpy of liquefaction
- 6) adsorption or desorption may only occur on or from exposed sites.

Below the saturation pressure P_0 , fractions of the surface are covered by layers randomly as in figure 2.7. The equilibrium condition between the vapor and the adsorbate of the first layer at a given pressure can be explained by Langmuir model:

$$\theta_0 \frac{P}{P_0} = \theta_1 \frac{P}{P_0} \frac{P_0}{P} \quad (2.4)$$

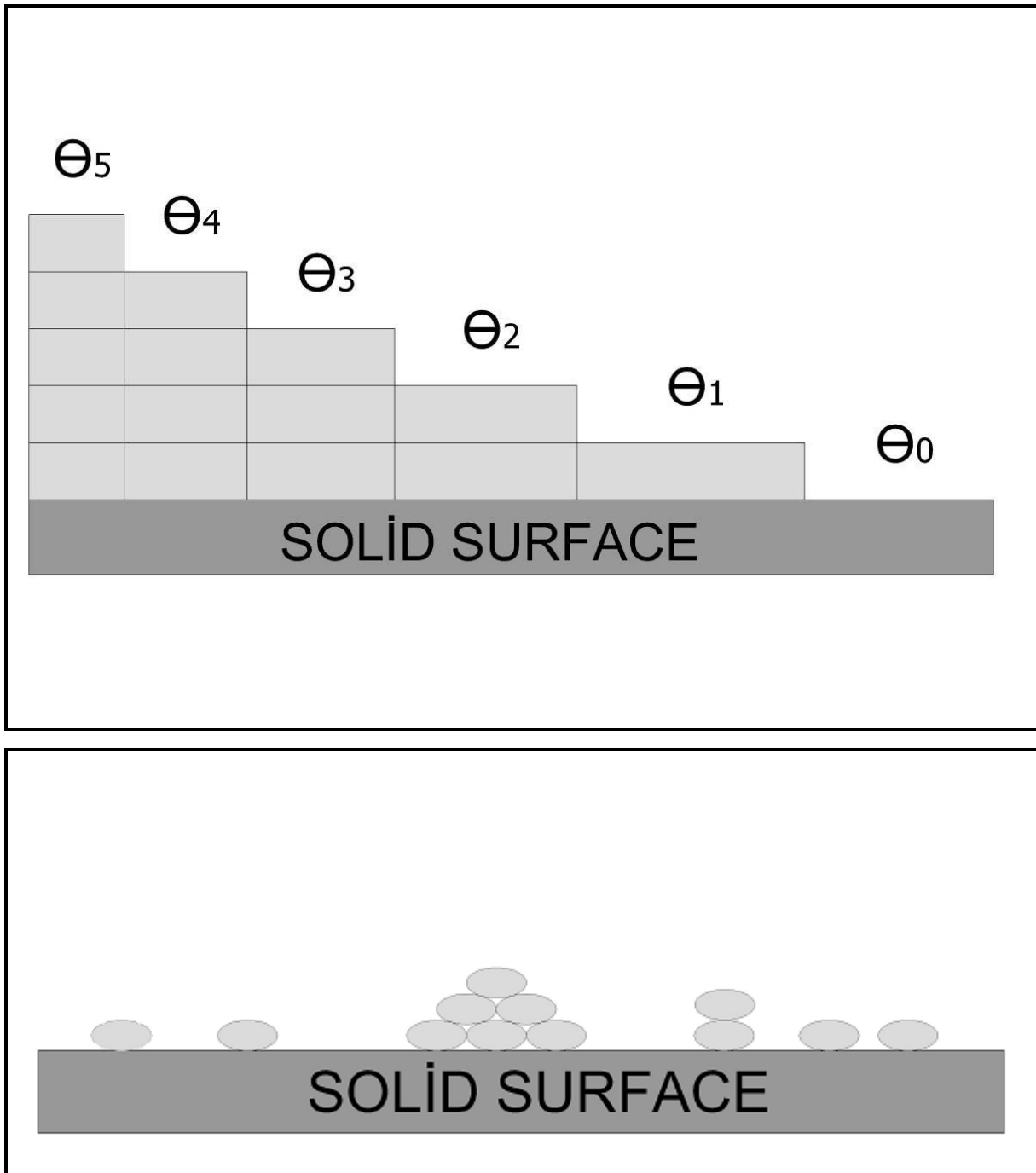


Figure 2.7 Adsorption process according to BET model and the the real model.

Then the adsorption to the following layers can be written as,

$$\theta_1 = \theta_2 \frac{K_2}{1 + K_2} \quad (2.5)$$

$$\theta_2 = \theta_3 \frac{K_3}{1 + K_3} \quad (2.6)$$

$$\theta_{i-1} = \theta_i \frac{K_i}{1 + K_i} \quad (2.7)$$

Where the sum of the fractional coverage equals to 1,

$$\theta_0 + \theta_1 + \theta_2 + \dots + \theta_i = 1 \quad (2.8)$$

and total number of molecules adsorbed at equilibrium can be written as,

$$n = n_0 \theta_0 + 2n_0 \theta_1 + 3n_0 \theta_2 + \dots + \infty n_0 \theta_\infty = n_0 (1\theta_0 + 2\theta_1 + \dots + \infty \theta_\infty) \quad (2.9)$$

The assumption is that the liquid state and the multilayer has an infinite thickness at $P/P_0=1$.

Taking the terms v , A , and E as constant and combining the above equations gives the linear form of the BET equation as:

$$\frac{P/P_0}{n_0(1 - P/P_0)} = \frac{1}{n_m C} + \frac{P/P_0 - 1}{n_m C} \left(\frac{C}{n_0} \right) \quad (2.10)$$

where C is,

$$C = \exp\left(\frac{E_1 - E_L}{RT}\right) \quad (2.11)$$

where E_1 is the heat of adsorption on the first layer and E_L is the heat of liquification of the adsorbed gas on all other layers. There are two steps to calculate the surface area by BET method. First $(P/P_0)/[n(1-P/P_0)]$ as a function of P/P_0 is plotted and from the slope, $s=(C-1)/n_m C$, and the intercept, $1/n_m C$, n_m is derived. In the second step, S_{tot} is calculated by the following formula,

$$S_{tot} = n_m a_{mol} \quad (2.12)$$

where a_{mol} is the surface area of one adsorbate molecule [40]

The BET equation is applicable for surface area analysis of nanoporous and mesoporous materials consisting of pores of wide pore diameter, but it is not applicable in case of microporous adsorbents [38].



The adsorption mechanism in mesopores is at lower relative temperatures as in case of adsorption on planar surfaces. First monolayer adsorption (A) occurs and it is followed by multilayer adsorption (B) until a critical film thickness is reached (C). After that capillary condensation occurs in the core of the pore (D). The pore liquid is separated from the bulk gas phase by a hemispherical meniscus. Pore evaporation occurs at a lower pressure than the condensation pressure by a receding meniscus(E) (figure 2.8). This difference between the

condensation and evaporation pressure of the pore liquid results in the formation of hysteresis loop in the isotherm.

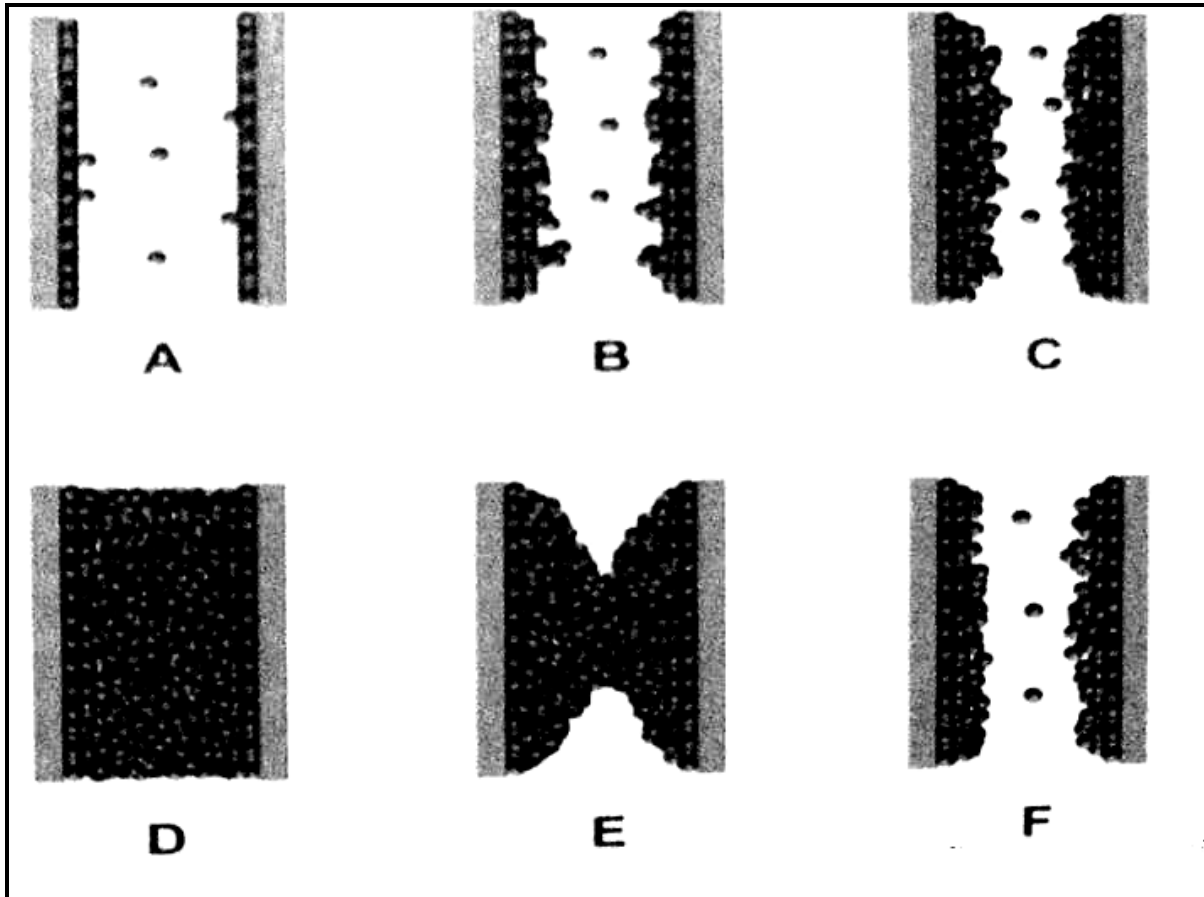
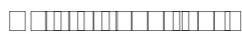


Figure. 2.8 Schematic representation of multilayer adsorption, pore condensation in a single cylindrical pore.



Kelvin equation can describe the condensation in pores that have a uniform shape and width. The relation between the equilibrium vapor pressure of a curved surface and equilibrium pressure of the same liquid on a plane surface can be written as:

$$\ln\left(\frac{P}{P_0}\right) = \frac{2\gamma \cos\theta}{rP_0} \quad (2.13)$$

where P is the equilibrium vapor pressure of the liquid in a pore of radius r , P_0 is the equilibrium pressure of that liquid on a plane surface and θ is the contact angle between the liquid phase and pore wall. Condensation takes place at a lower pressure in a mesopore because the overlapping potentials of the walls which overcome the translation energy of an

adsorbate molecule. Condensation in smaller pores will occur first with the increasing relative pressure and will continue to occur in larger pores until the radius reaches infinity (plane surface). Before condensation adsorption starts on the pore wall so when evaporation of the center core occurs an adsorbed film remains on the pore wall. The radius given by Kelvin equation, r_K is not the actual radius, r but the core radius. The sum of the Kelvin radius and thickness of the adsorbed layer, t gives the actual radius. The relationship is shown in figure 2.9.

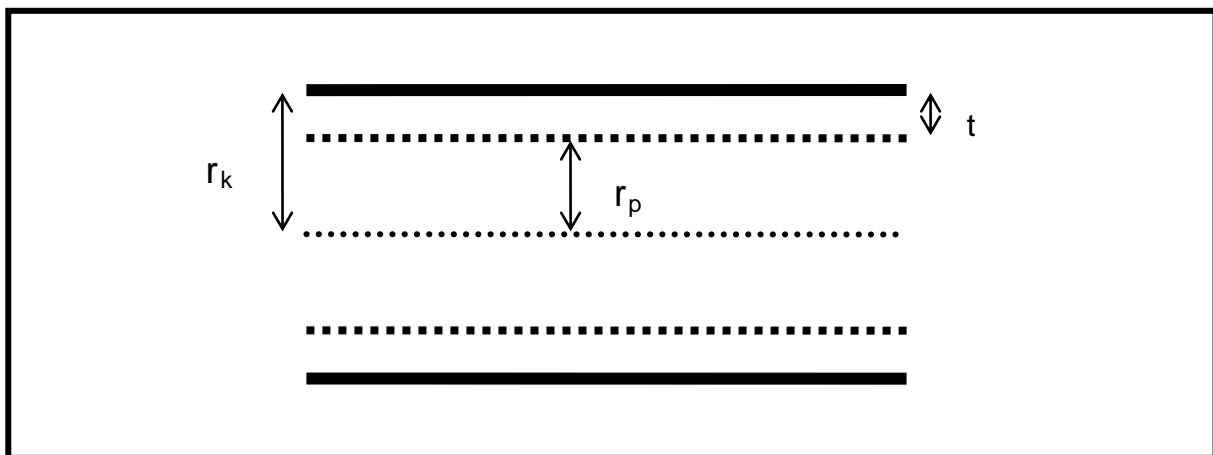


Figure 2.9 Relationship of r_K , t and r in a cylindrical pore.

This equation serves as the basis for many methods for mesopore analysis including the r_K method (BJH) method which is the most commonly used method for pore analysis of mesoporous materials. The desorption branch of the hysteresis loop of the isotherm for the sorbent is used in this method. This is because the desorption process is more thermodynamically stable. The assumptions for this method are as follows [41],

- All pores are non-intersecting, cylindrical pores,
- Hemispherical meniscus with zero contact angle, or complete wetting,
- The simple Kelvin equation is applicable,
- Validity of the correction for multilayer adsorption.

2.5.4 Transmission Electron Microscopy (TEM)

The resolution of the images that we are able to see with a light microscope is limited by the wavelength of light. The transmission electron microscope operates on the same basic principles as the light microscope but uses electrons instead of light. By using electrons the limit of resolution of the microscope lowers to the very much lower wavelength of electrons.

It is possible to see objects to the order of a few angstroms. Such high resolutions made the TEM a valuable tool in both materials sciences and biological sciences.

A TEM is composed of several components, which include a vacuum system in which the electrons travel an electron emission source for generation of the electron stream, a series of electromagnetic lenses, as well as electrostatic plates. The latter two allow the operator to guide and manipulate the beam as required.

The illumination is provided by an electron gun while the lenses are all electromagnetic. The remaining necessary components are a viewing screen which is usually a simple layer of electron fluorescent material, viewed through a lead glass window, and a camera, which must work in the vacuum within the microscope. These components are assembled into a vertical 'microscope column' which is shown in figure 2.10 [42].

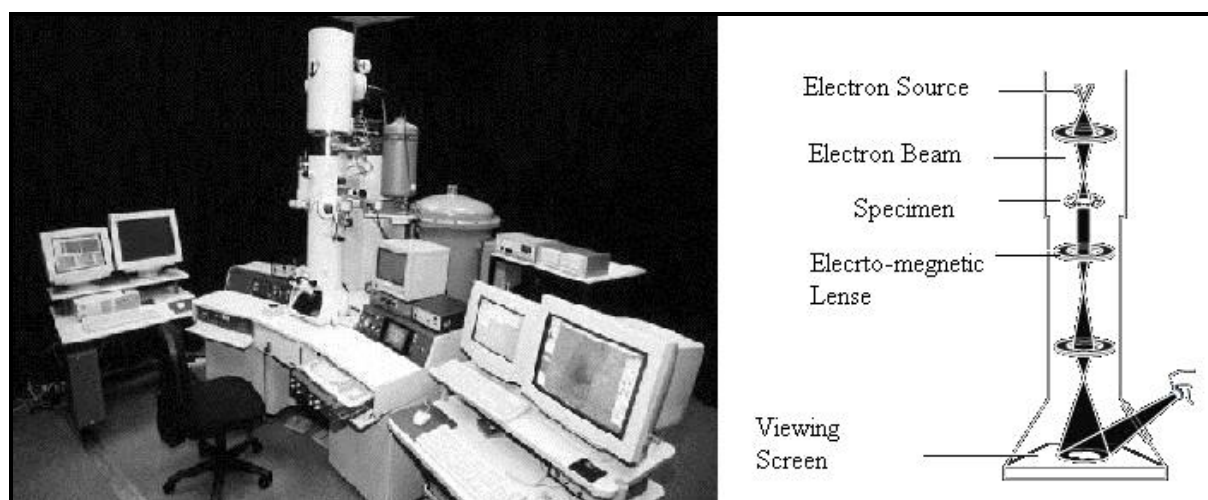


Figure 2.10 Transmission electron microscopy.

The microstructures of carbon black - silica composite aerogels were investigated by transmission electron microscopy (TEM). Specimens for TEM examination were prepared by carefully crushing the composite samples with a mortar and pestle set and then dipping copper mesh grids coated with holey carbon films (Quantifoil Micro Tools GmbH) into the powder. The specimens were examined in a JEOL 2010 FasTEM operating at 200 kV. This instrument is equipped with a high-resolution objective lens pole-piece (spherical aberration coefficient $C_s = 0.5\text{mm}$) giving a point-to-point resolution of $<0.19\text{ nm}$ in phase contrast images. Chemical microanalysis was performed in situ using an EDAX Phoenix atmospheric thin window energy-dispersive X-ray spectrometer (EDXS).

2.5.5 FTIR and Raman spectrometry

The characters of the silica and carbon in the composites were assessed using FTIR and Raman spectrometry, respectively. Infrared spectroscopy and Raman spectroscopy are complementary techniques, because the selection rules are different. For example, homonuclear diatomic molecules do not have an infrared absorption spectrum, because they have no dipole moment, but do have a Raman spectrum, because stretching and contraction of the bond changes the interactions between electrons and nuclei, thereby changing the molecular polarizability. For highly symmetric polyatomic molecules possessing a center of inversion (such as benzene) it is observed that bands that are active in the IR spectrum are not active in the Raman spectrum (and vice-versa). In molecules with little or no symmetry, modes are likely to be active in both infrared and Raman spectroscopy.

The FTIR samples were prepared as KBr pellets containing ~1.0 wt. % of the composite powder. Spectra were acquired from these pellets using the transmittance method in a 2x-Nicolet Magna 560 FTIR spectrometer. Raman spectra were obtained in the range of 600-2000 cm^{-1} from composite powder samples using Renishaw Ramascope Micro-Raman spectrometer equipped with a 514.5nm argon laser.

Chapter 3

RESULTS AND DISCUSSIONS

3.1 TEOS Concentration Effect

A series of silica aerogels were synthesized to investigate the effect of reactant concentrations on the properties. In the first set of experiments, TEOS:ethanol weight ratio was varied from 2:10 to 7:10. A further increase in the TEOS concentration was not possible. The solution with 70 % TEOS by weight, is close to the miscibility line of the ternary phase diagram of the system TEOS-ethanol-water at 298K shown in figure 1.1. The solution becomes a single phase with the addition of HCl. For concentrations higher than 70 % wt, the solution was not miscible even after HCl addition. Another difficulty in solutions with high TEOS concentration occurs in the base addition step. It becomes easier to form precipitates during the addition of base catalyst. One way to avoid this problem is to use a dilute base catalyst solution. However, this requires the addition of a higher amount of base catalyst solution into the sol which makes it difficult to target the desired sol concentration. Adding the base catalyst slowly is another way to overcome this problem, but as the TEOS concentration increases gelation time decreases which may result in gelation during catalyst addition. Therefore, the concentration and addition rate of the base catalyst was optimized. After four days of solvent exchange with ethanol, these gels were extracted with supercritical carbon dioxide.

The results presented in Table 3.1 show that increasing the TEOS concentration in the sol resulted in a slight increase in the densities of the aerogels and a decrease in the shrinkage values. One can expect the densities of the aerogels to increase more than observed due to higher amount of silica source within the same mold. This behavior can be explained by the differences in the shrinkage values of the samples. In order to obtain aerogels with low densities, it is not enough to start with a dilute sol but shrinkage should also be minimized.

Table 3.1. TEOS Concentration effect.

TEOS Conc. (wt %)	Density (g / cc)	Shrinkage (%)	BJH Pore Vol. (cc/g)	BJH Pore Diameter (nm)
20	0.23	38	2.86	13.5
30	0.26	32	2.16	11.1
40	0.27	27	1.87	9.8
50	0.36	27	1.64	7.3
60	0.32	24	1.66	7.1
70	0.33	23	1.95	7.5

Before the BET analysis, the samples were degassed at 573 K for 150 min. Figure 3.1 shows the pore size distributions of silica aerogels produced from solutions with different TEOS concentrations. As the TEOS concentration increased, the pore size distribution became narrower and the average pore size shifted to smaller pore diameters. This behavior is presented more clearly in Figure 3.2 which shows that the average pore diameter decreased up to 50 wt% TEOS concentration and then stayed almost constant with further increases in the TEOS concentration. On the other hand, pore volumes of the samples decreased up to 50 wt% TEOS concentration and then started to increase by further increases of TEOS concentration (Figure 3.4). The changes in the pore size distributions of the silica aerogels that were synthesized with different TEOS: Ethanol ratios can be attributed to the differences in the strengths of their silica networks. In the experiments, the ratios of the reactants, TEOS; water; the catalysts, were kept constant and the alcohol concentration was the only parameter which was varied to obtain a higher solid content within the same volume. This led to higher concentrations of hydrolyzed silica source available for the condensation step. This increase in the concentration of partially condensed silica decreased the time to reach the gelation point regardless of the reaction rate. The denser the alcogel the stronger its structure becomes. This allows the gels to resist the capillary forces during drying. It can be expected that 20 wt% gels smaller pores collapsed during drying and formed bigger pores which shifts its pore size distribution curves to larger pore sizes.

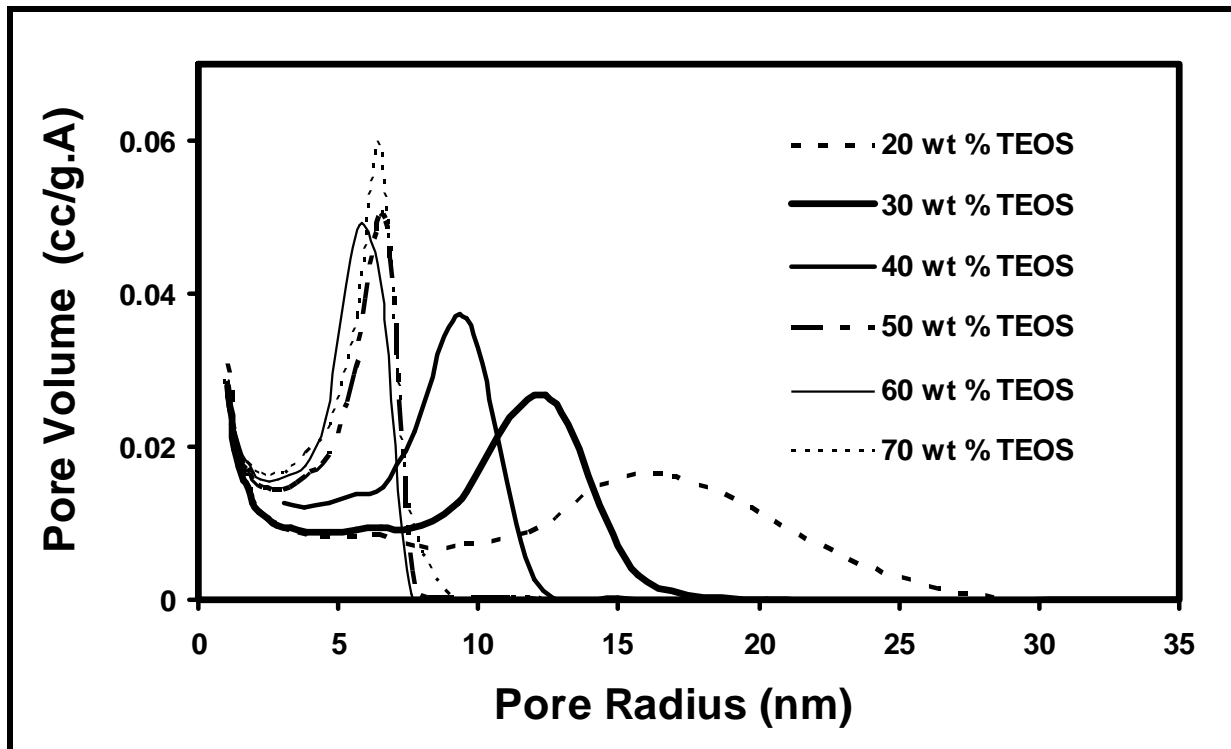


Figure 3.1 Pore size distributions of aerogels with different TEOS concentrations.

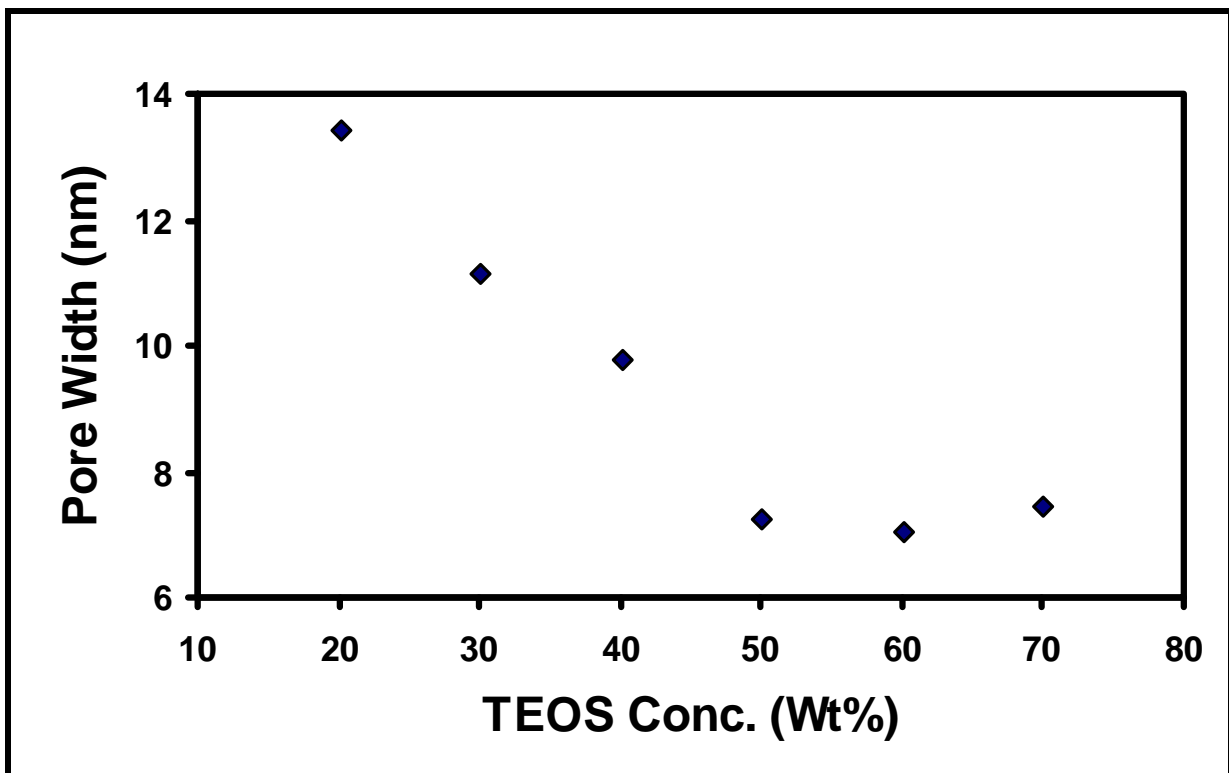


Figure 3.2 TEOS concentration effect on average pore size.

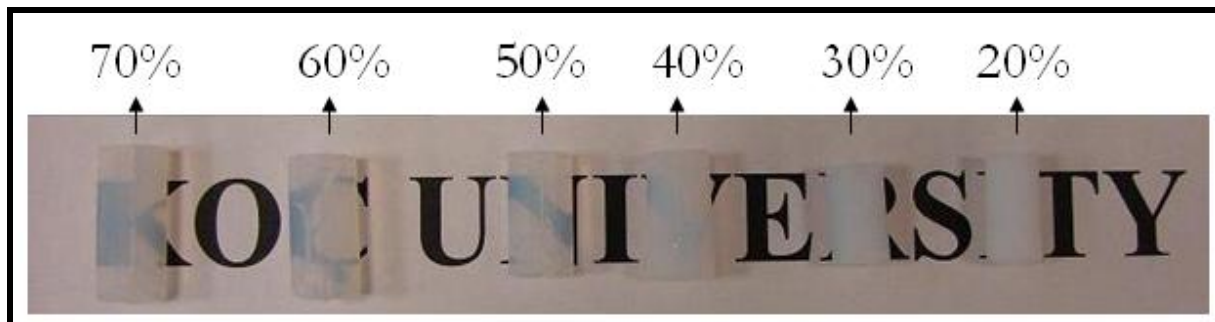


Figure 3.3 Images of silica aerogels having different TEOS concentrations given as wt% to sol.

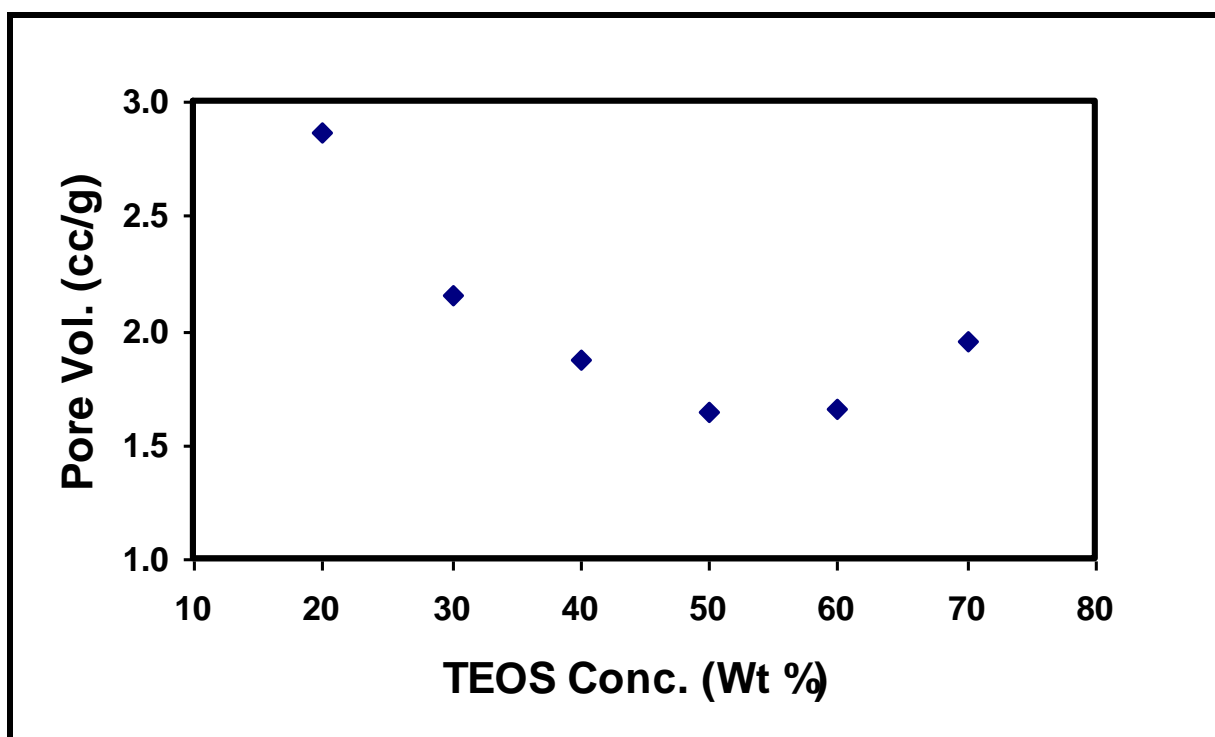


Figure 3.4 TEOS concentration effect on pore volume.

Aerogels appear slightly bluish against a dark background because of Rayleigh Scattering. Two types of scattering occur in aerogels which are bulk scattering and surface scattering. Rayleigh scattering is the scattering effect observed by small dust particles in the atmosphere. The actual entity that causes scattering, called the scattering center, can be as small as a single large molecule with an inherent inhomogeneity or clusters of small molecules arranged in a non-uniform way. When the size of the scattering center is similar to

the wavelength of the incident light, scattering becomes more effective. However, when scattering centers are smaller in size than the wavelength of the incident light, scattering is much less effective.

In silica aerogels, the primary particles have a diameter of ~2-5 nm, and do not contribute significantly to the observed scattering. However, scattering does not necessarily arise from solid structures. In silica aerogels, a network of pores can act themselves as scattering centers. After investigations on optical properties of silica aerogels, it has been found that the quantity of bulk Rayleigh Scattering in silica aerogel is related to density and pore size which are based on chemistry of the gel formation. Surface scattering is not related to gel formation chemistry but depends on the nature and physical characteristics of the reactors vessel including vessel walls, mechanical vibration and possibly, dust.

According to previous works, transparency increased with increasing bulk density and the more important parameter for high transparency is the particle size and pore size minimization [6]. In the light of this information by looking at table 3.1, one can expect the 60 wt% TEOS concentrated sample having a minimum density and pore size is the best for applications where transparency is important. It can be seen from Figure 3.3 that the transparency of the samples improved significantly with increasing TEOS concentration. There is a sharp change from 40 wt% sample to 50 wt% sample. This is a result of the shift of the pore size distribution curves to smaller pore diameters with a sharper peak

3.2 Aging Effect

In the second set of experiments, the effects of the aging solution on the properties of the gels were investigated. Aging can be identified as the period while further rearrangement reactions occur after gelation point. During aging, smaller particles dissolve and re-precipitate on larger ones which cause small particles to diminish in quantity and small pores to be filled. The nature of the aging solutions and temperature affect the reactions occurring in this period. The aging experiments were carried out with the 60 wt% sample to further improve the transparency and mechanical strength of the samples. Silica gels obtained from the same sol were aged in TEOS/Ethanol, Water/Ethanol and pure ethanol solutions for 20 hours at different temperatures. They were then placed into pure ethanol for a certain period of time for solvent exchange.

Table 3.2 shows the effect of the aging condition on the densities and shrinkage values of the aerogels. According to these results, aging the gels in TEOS/Ethanol solution at room temperature did not have an effect on the amount of shrinkage when compared to non - aged samples. When temperature increased to 323K shrinkage decreased from 23 to 18% which is not a significant decrease. On the other hand, water had such a strengthening effect on the gel structure that it decreased shrinkage of the samples to 11%. Transparent and monolithic aerogels with such lowered shrinkage values were obtained by aging the gels in 50% water-ethanol solution at 323K. The results are also in agreement with the observations of G. Reichenauer et al. who showed that using water as the aging solution lead to gels that are mechanically stronger and also that have less external and micropore surface area which decrease shrinkage during drying [22].

Table 3.2 Effect of Aging Conditions.

Aging Temp. (K)	Aging solvent	Density (g/cc)	Shrinkage (%)	BJH Pore Vol. (cc/g)	BET Surface Area (m²/g)	BJH Pore Diameter (nm)
373	Ethanol-water	0.16	11	4.50	662	22.1
323	Ethanol-Water	0.19	11	4.25	1029	14.0
323	Ethanol-TEOS	0.27	18	2.05	916	8.3
298	Ethanol-TEOS	0.31	22	1.82	870	7.9
298	Ethanol	0.32	23	1.66	900	7.0

Pore size distributions of silica aerogels which were aged in different solutions at different temperatures are given in Figure 3.5. Aging the gels in TEOS/Ethanol solution did not have a considerable effect on pore size distribution when compared to the gel aged in ethanol before drying. When the gel is aged in Water/Ethanol solution for 20 hours, a significant increase was observed in the pore volume accompanied by an increase of the average pore size. The increase in the pore volumes from 1.66 to 4.50 can be explained

mainly by the difference in the shrinkage values of these samples which is the result of the strengthening of the gel network during aging. The decrease in the surface area from 1029 to 662 can be attributed to the decrease in the ratio of small particles to the larger ones when the density is similar. But the surface areas of the TEOS aged and water aged samples can not be compared because of the large difference between their shrinkage values.

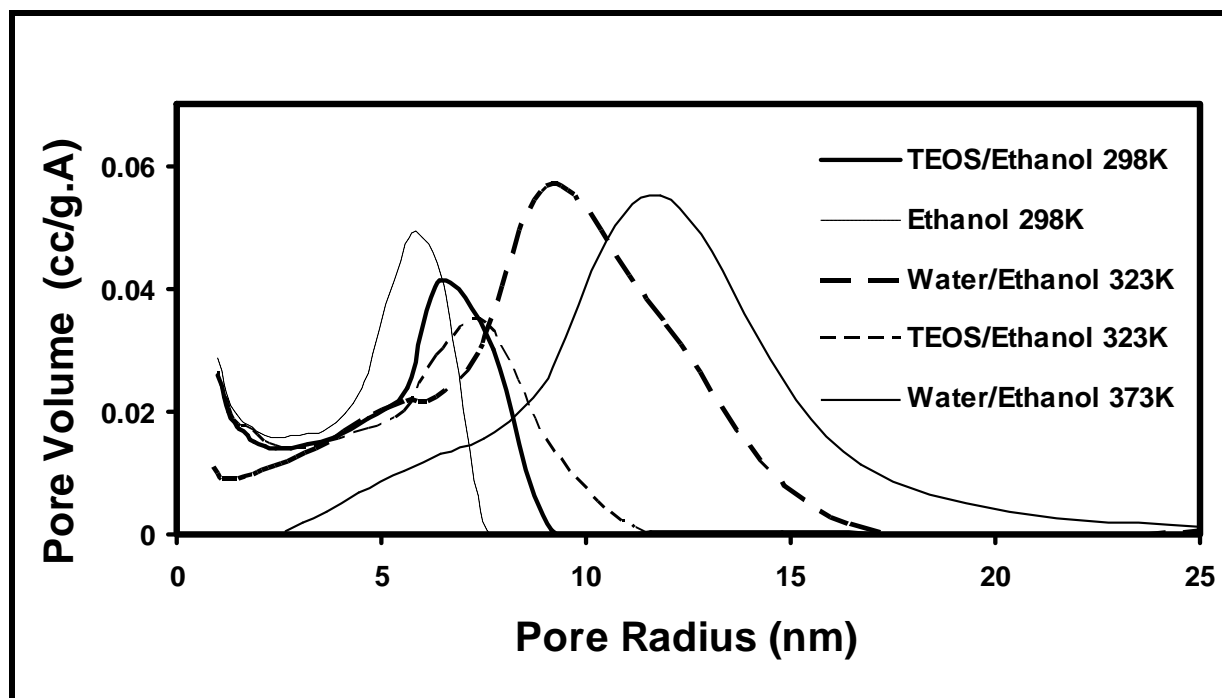


Figure 3.5 Pore size distributions of silica aerogels aged in different solvents.

Figure 3.6 shows the TGA of two aerogel samples that have been prepared by identical synthesis and drying procedures. One of them was heat treated in a tube furnace at 673K for 4h, and the other one was not heat treated. TGA was performed in an oxygen atmosphere. The 6 % weight loss observed up to 100⁰ C is presumably due to loss of adsorbed water. The same amount of loss observed in the heat treated sample in the same temperature range shows that the samples adsorb water 6% of its weight fast. The loss around 300⁰ C is believed to be due to the unreacted TEOS or some organic end groups such as CH₃. Once these groups are released by heat treatment the sample does not lose weight at these temperatures any more. The samples are stable up to 1000⁰ C and do not crack.

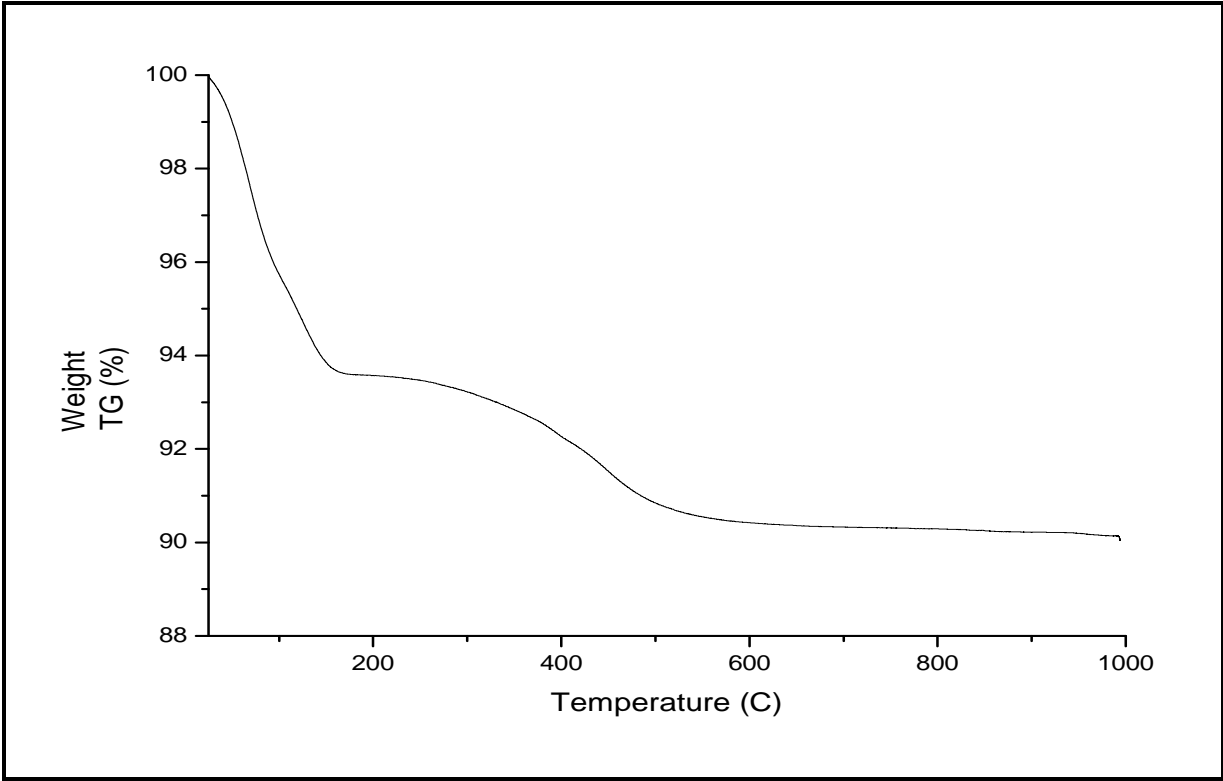
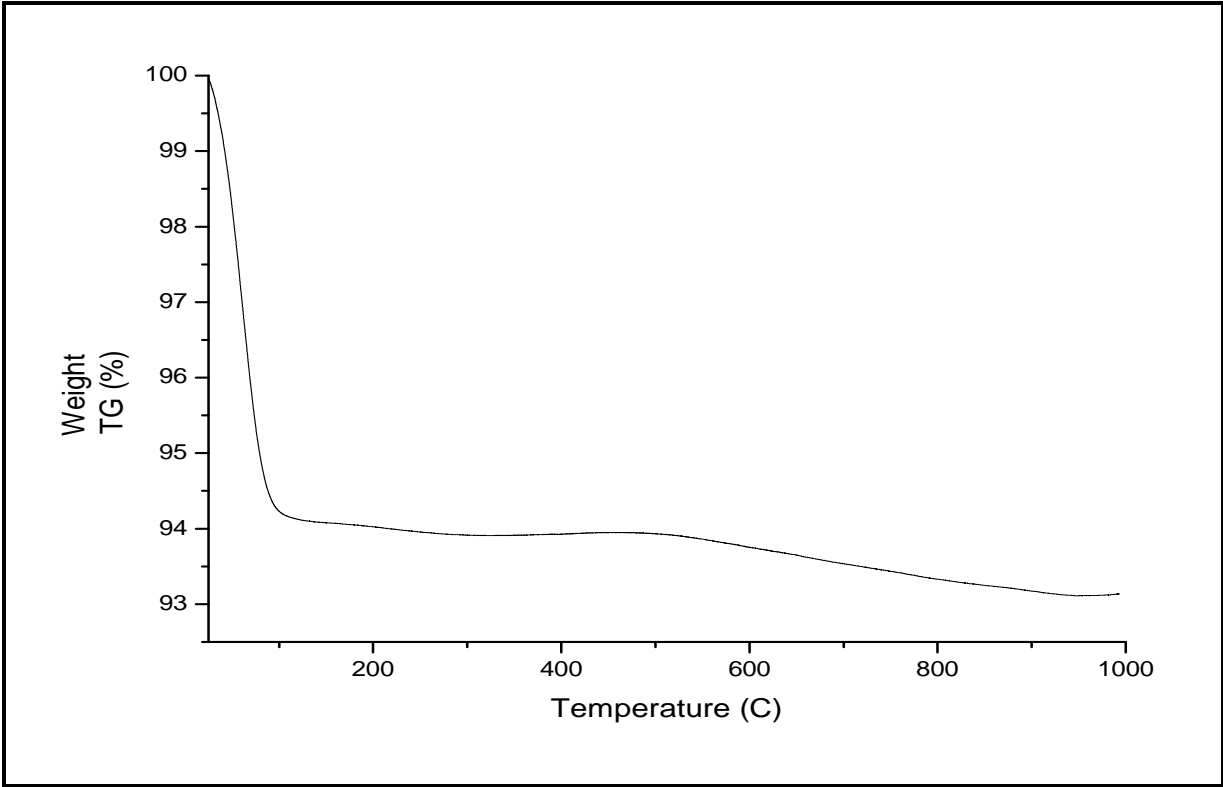


Figure 3.6 TGA results of 2 silica aerogel samples a) heat treated before TGA analysis, b)TGA analysis directly after drying.

3.3 Carbon Black Silica Aerogel Composites

Composite aerogels were synthesized using solutions with 50 wt% TEOS concentration. The main reason behind selecting 50 wt% TEOS concentration was the decrease of gelation time with increasing TEOS concentration. Above a TEOS concentration of 50 wt%, there was not enough time to mix the sol with carbon black and transfer it into the mold as gelation occurred during mixing. However when a more dilute sol was used, the increase in the gelation time resulted in a concentration gradient of carbon throughout the mold.

Carbon – silica composite aerogels were prepared either by adding the carbon before gelation or making a powdered composite material by physically mixing the carbon black powder with aerogel powder. It was observed that addition of carbon black to the sol after base catalyst addition did not change the gelation time. By this observation, it can be said that it did not affect the rate of condensation reaction in a noticeable way. On the other hand our gelation time is a short time to be able to see a lower effect. Further studies can be performed using sols with a lower TEOS concentration in order to investigate this effect deeply.

During drying no differences was observed with silica aerogel drying. Carbon black had a strengthening effect on the resulting aerogels and the composite aerogels were less fragile. On the other hand, when we used the same drying conditions and time, carbon black addition did not decrease shrinkage of the samples during drying.

The amount of carbon black was calculated first theoretically by the help of our background on silica aerogels. It was observed that conversion of TEOS to silica was not 100% from the silica aerogel mass results and the TEOS amounts used in the synthesis of the silica aerogels. The carbon black wt% of the resulting aerogels were desired to be 0.3, 1, 2.5 and 4.5 wt% and the calculations were done using the expected silica mass from the known amount of TEOS used with the conversion ratio background from the silica aerogel experiments. The resulting composite aerogels were pretty much the same as the desired weight % values which were 0.34, 1.08, 2.29 and 4.5 wt%.

Table 3.3 summarizes the effect of carbon black weight percentage on the pore properties of composite aerogels. Addition of a small amount of carbon black resulted in a slight decrease in the pore volume from 5.3 to 3.9 cc/g and average pore diameter from 16.8

to 13.9 nm. Increasing the carbon black ratio brought forth a slight increase in pore volume up to 4.6 cc/g and in average pore diameter up to 17 nm.

Table 3.3 Properties of carbon black - silica composite aerogels

Carbon content (Wt %)	Apparent density (g/cc)	BET Surface Area (m²/g)	BJH Pore Vol. (cc/g)	BJH Pore Diameter (nm)
0	0.14	1083	5.30	16.8
0.34	0.15	989	3.92	13.9
1.08	0.22	1067	4.49	14.7
2.29	0.15	978	4.61	16.1
4.50	0.14	909	4.63	17.4

On the other hand, the surface area of the samples were not affected by the carbon black amount. It first decreases from 1083 m²/g to 989 m²/g with 0.34 wt% carbon black than increase to 1067m²/g with 1.08 wt% carbon black. Increasing the carbon black amount to 4.5 wt% again decreased the surface area to 909 m²/g.

Figure 3.7 shows the pore size distributions of the composite aerogels. As the carbon black content in the aerogel increases, the pore size distribution curves slightly shifts to higher pore diameters with different intensities. The information given in Table 3.3 is plotted separately as follows; Figure 3.8 shows the pore volumes, Figure 3.9 shows the pore diameters and Figure 3.10 shows the surface area versus carbon black weight percentages in the composite aerogels. With these figures it is clear that at first the pore volumes and the pore diameters decrease with addition of a small amount of carbon black to the sol and then increase with a decreasing slope. As shown in Figure 3.10, there is not a distinct relationship between carbon black amount and BET surface area.

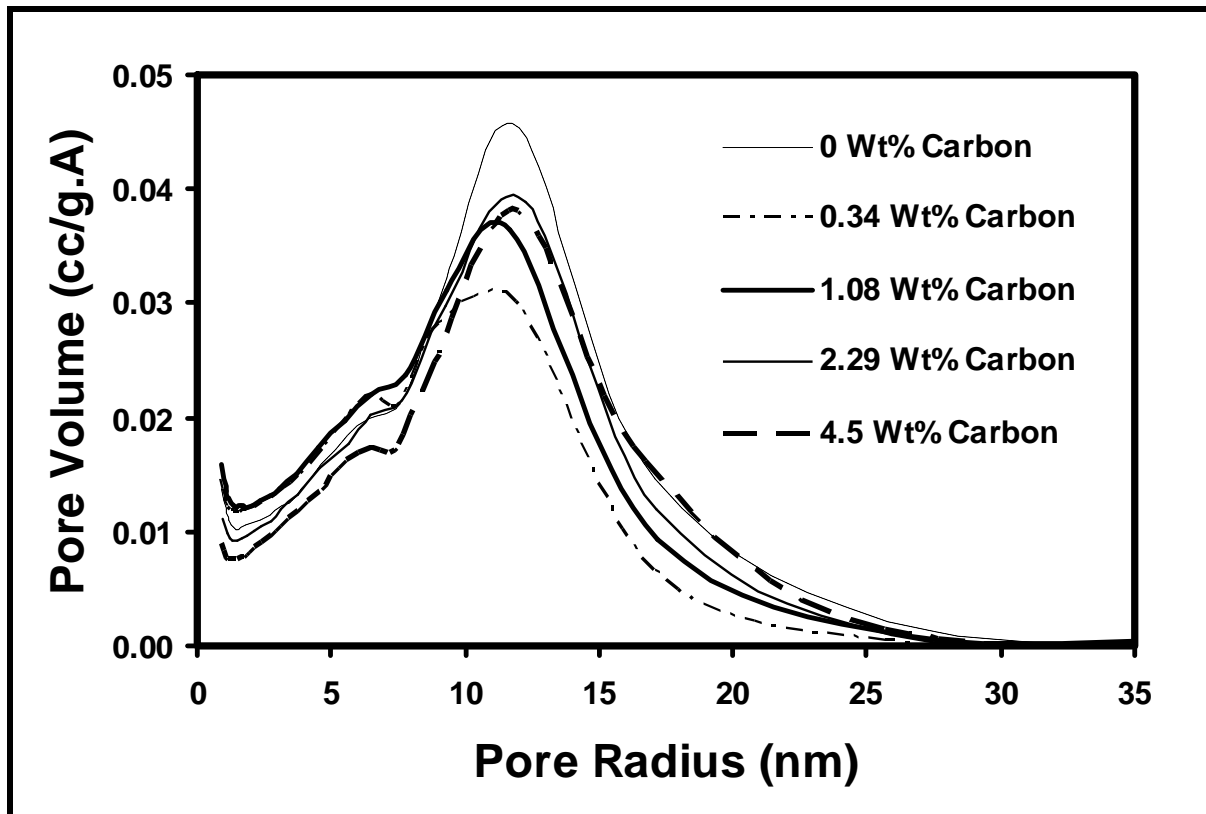


Figure 3.7 Pore size distributions of carbon-silica composite aerogels with different carbon contents

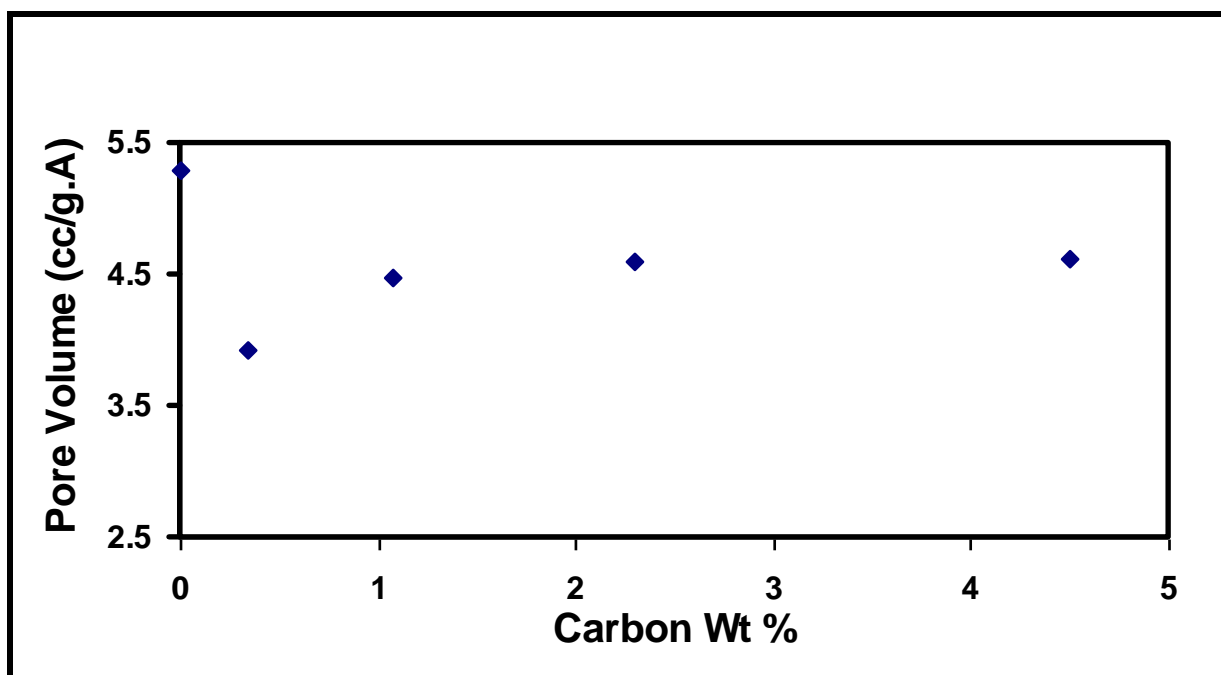


Figure 3.8 Carbon wt% effect on pore volume of composite aerogels

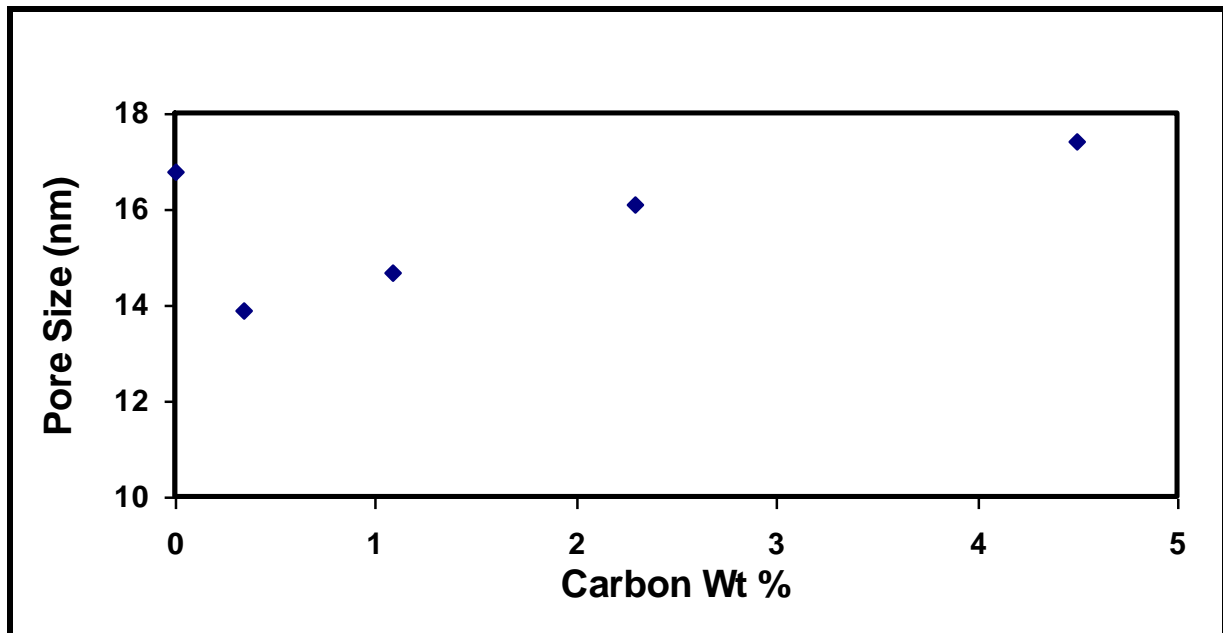


Figure 3.9 Carbon wt% effect on pore width of composite aerogels

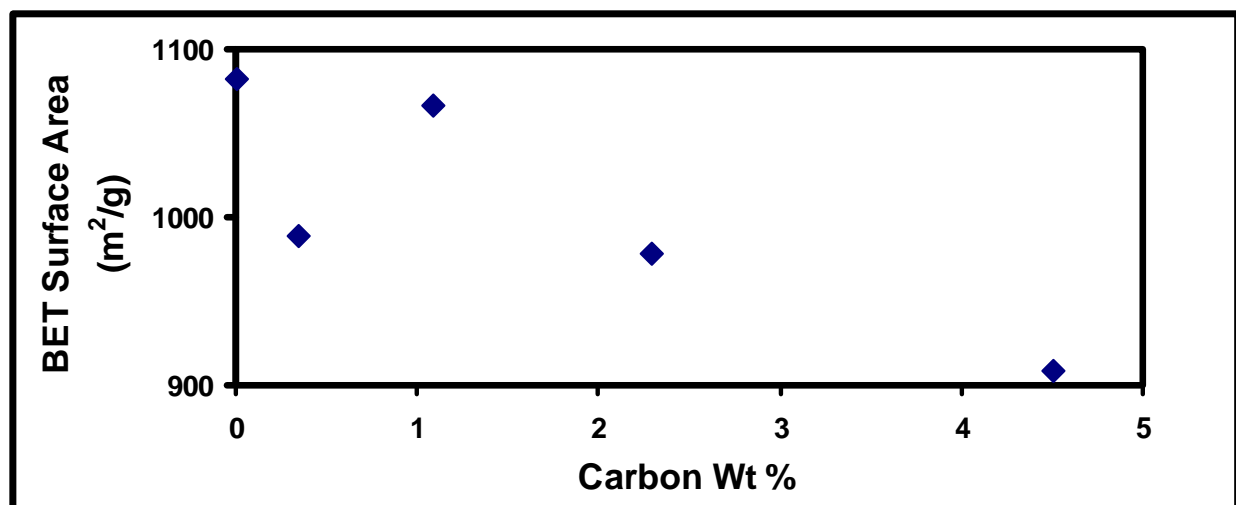


Figure 3.10 Carbon wt% effect on BET surface area of composite aerogels

Considering all of the nitrogen adsorption physisorption measurements, the t-plot micropore volumes were nearly zero, indicating that the micropores are not present or are very low that is out of the detection limit. It is possible to calculate the pore volumes of the aerogels using their densities with the given correlations in section 2.5.1. The apparent density values given in tables 3.1, 3.2 and 3.3 were calculated with the radius, length and weight data that were measured just after the drying step of the gels. These density values were not used

for expected pore volume calculations because of the degas step performed before the nitrogen adsorption physisorption measurements. The aerogel shrinks more and loose weight during this step which changes their densities. Especially shrinkage caused by the degas step which was discussed in section 2.5.3 results in an increase in the density values of the samples. It is inevitable to use the density values after degas for calculation of expected pore volume. It was not possible to perform the degas experiment for each monolith to observe the amount of shrinkage because of the limitations of the dimensions of the degas instrument and our monolithic samples. We performed a few experiments with some monolithic samples and obtained an average shrinkage value. The dimension and weight values corrected to the values after degas and the corrected values were used in the calculation of the densities after degas and expected pore volumes of the aerogel samples. The expected pore volumes were calculated the formula (2.2) given in section 2.5.1. The density values of the silica aerogels before and after degas is given in table 3.4. It can be observed from the expected pore volumes and the measured pore volumes by BJH method in table 3.4 have no significant differences so it can be concluded that the aerogels synthesized by this method had no macropores as well. Both silica aerogels and the carbon black silica composite aerogels synthesized were strictly mesoporous materials.

Table 3.4 The densities and calculated pore volumes of silica aerogel samples after and before degas.

TEOS Conc. (Wt %)	Density Before degas (g / cc)	Density After degas (g/cc)	Pore Vol. Calculated (cc/g)	Pore Vol. BJH (cc/g)
20	0.23	0.32	2.65	2.86
30	0.26	0.36	2.56	2.16
40	0.27	0.37	2.47	1.87
50	0.36	0.50	1.96	1.64
60	0.32	0.45	2.14	1.66
70	0.33	0.45	2.11	1.95

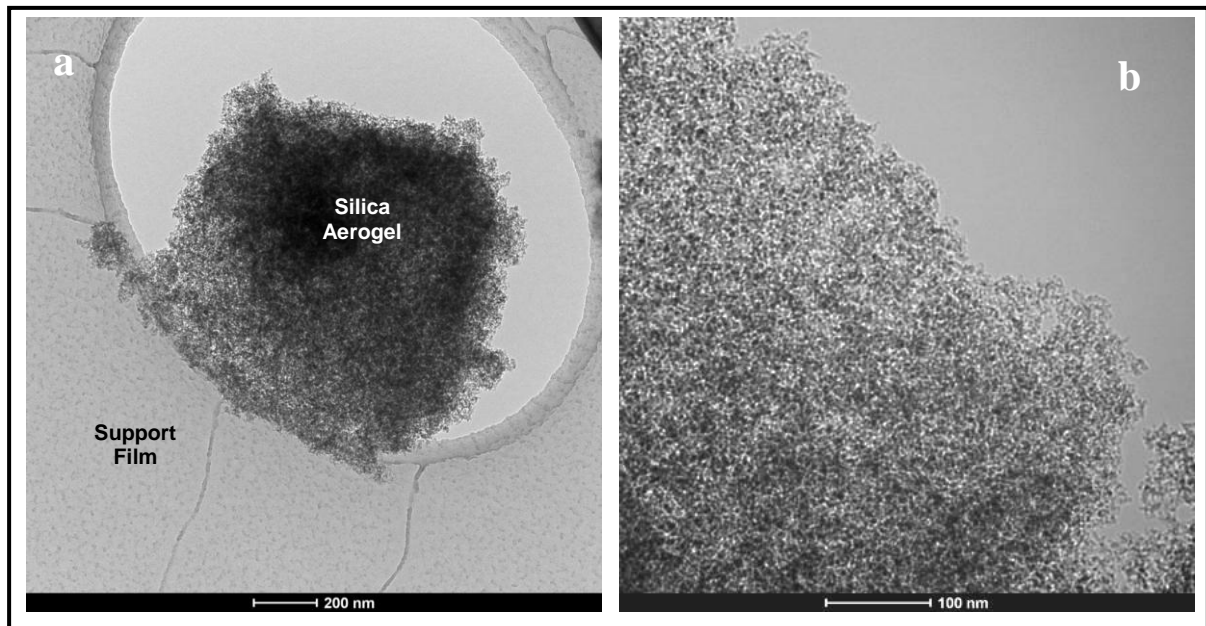


Figure 3.11 Bright field TEM images obtained from the composite with 0.34 wt. % carbon

The general morphology of composite aerogels having different carbon contents were observed using transmission electron microscopy. In the 0.34 and 1.08 wt.% carbon composites it was very difficult to locate the carbon. Typical images obtained from the 0.34 wt. % carbon composite are shown in figure 3.11. Figure 3.11(a) is an image of a 1 μ m fragment of the composite suspended on the edge of a hole in the carbon support film on the TEM grid, and figure 3.11(b) is a higher magnification image from the edge of another fragment. These images show a uniform porous structure and closely resemble those obtained from pure silica aerogel samples.

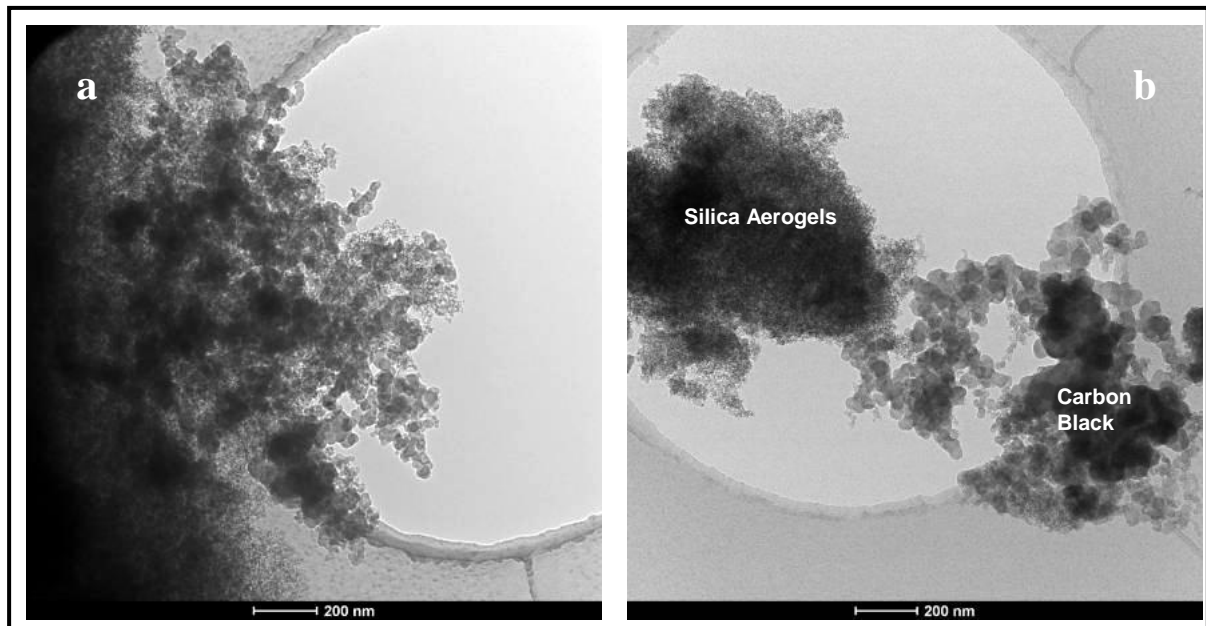


Figure 3.12 Bright field TEM images obtained from the composite with 4.50 wt. % carbon

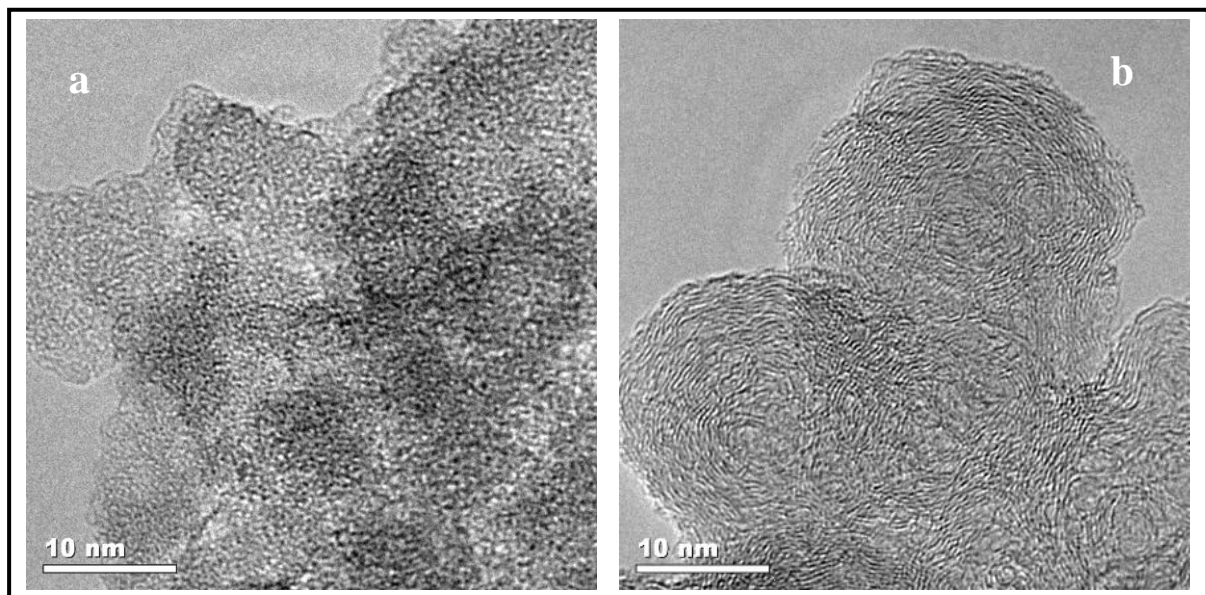


Figure 3.13 High-resolution TEM images obtained from the composite with 4.50 wt. % carbon showing the structural detail in regions of: (a) silica aerogel; (b) carbon black

In the 2.29 and 4.50 wt.% carbon composites, however, it was much easier to identify the carbon black phase; this appeared as aggregates a few hundred nanometers across consisting of structural units 20-40 nm in diameter. Examples of TEM images obtained from the 4.50 wt.% carbon composite are shown in Figure 3.12. Figure 3.12(a) is a typical image

of a composite fragment in which the contrast from the carbon black is superposed upon that from the silica aerogel. Figure 3.12(b) is an atypical area in which separate fragments of the two phases can be seen and so the distinction is particularly clear; EDXS spectra were used to show that the fragment on the left-hand side of the image with the finer structure is silica aerogel while the aggregate on the right is almost pure carbon black. The differences in the structure of these regions were revealed in more detail by phase contrast high-resolution TEM images such as those shown in Figure 3.13. The contrast from the silica aerogel (Figure 3.13(a)) is consistent that expected for a fully amorphous SiO_2 structure. By comparing many such images we deduce that the aerogel is 3D framework structure comprised of features 5-10 nm in diameter, although the framework is obscured somewhat by projection effects in individual high-resolution TEM images. The structural units in the carbon black are larger (20-40nm) and more well-defined so the high-resolution TEM images such as Figure 3.13(b) reveal the internal structure of the units more clearly.

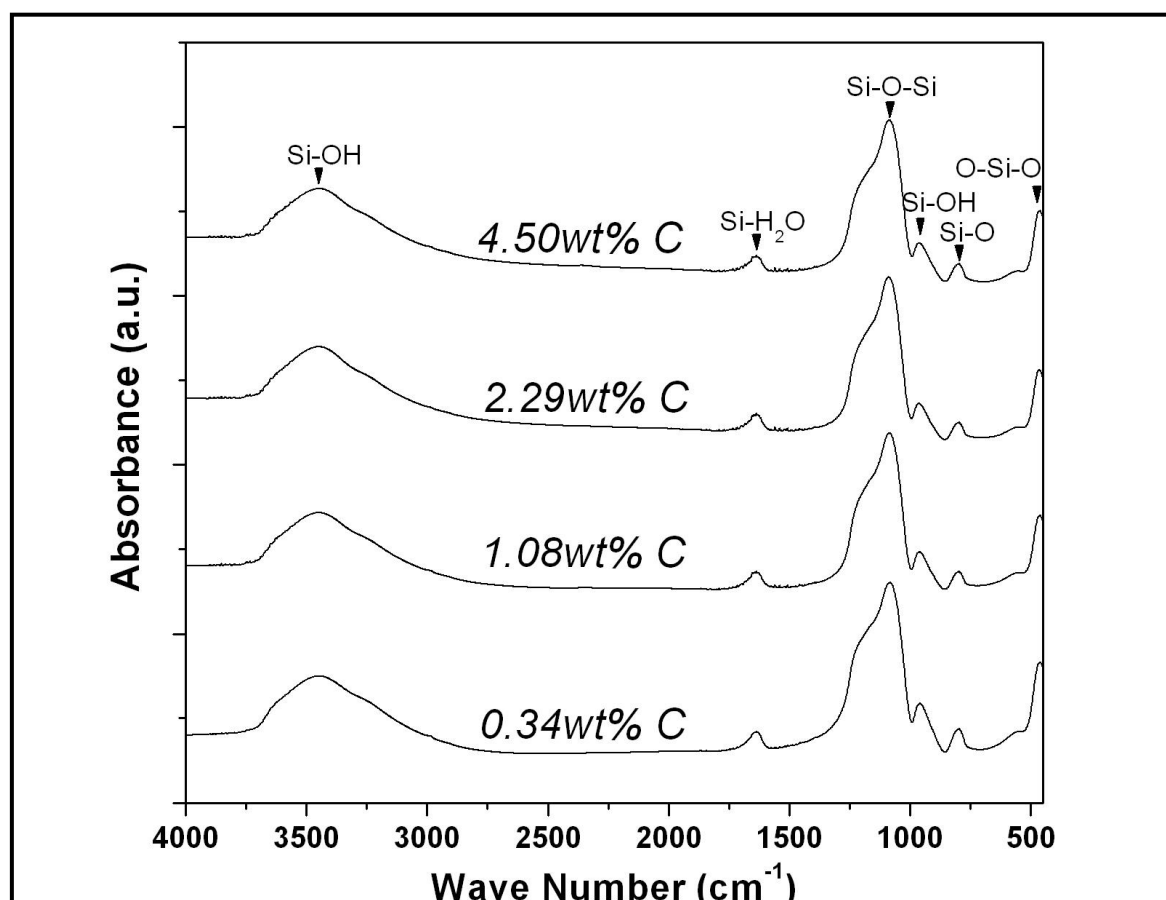


Figure 3.14 Infra-red transmittance spectra obtained from the carbon black - silica aerogel composites showing no effect of carbon content on oscillation modes

TEM data suggest that the silica and carbon are phase-separated in the composites, and it was confirmed by the FTIR and Raman data that silica and carbon were not mixed on a molecular level in the composites. The IR transmittance spectra obtained from the composite samples with different carbon contents are shown in Figure 3.14. The adsorption bands in the spectra show distinctive peaks at 3450 and 950 cm^{-1} which represent Si–OH stretching; a peak at 1635 cm^{-1} corresponding to Si–H₂O flexion; peaks at 1080, 800, 561 and 455 cm^{-1} for the Si–O–Si, Si–OH, Si–O and O–Si–O vibration bands, respectively which are typical for silica aerogels. It is clear from these spectra that there are no significant changes in the positions, shapes or relative intensities of these peaks; this indicates that the presence of up to 4.5 wt. % carbon black in these composites does not modify the bonding characteristics of the silica aerogels significantly.

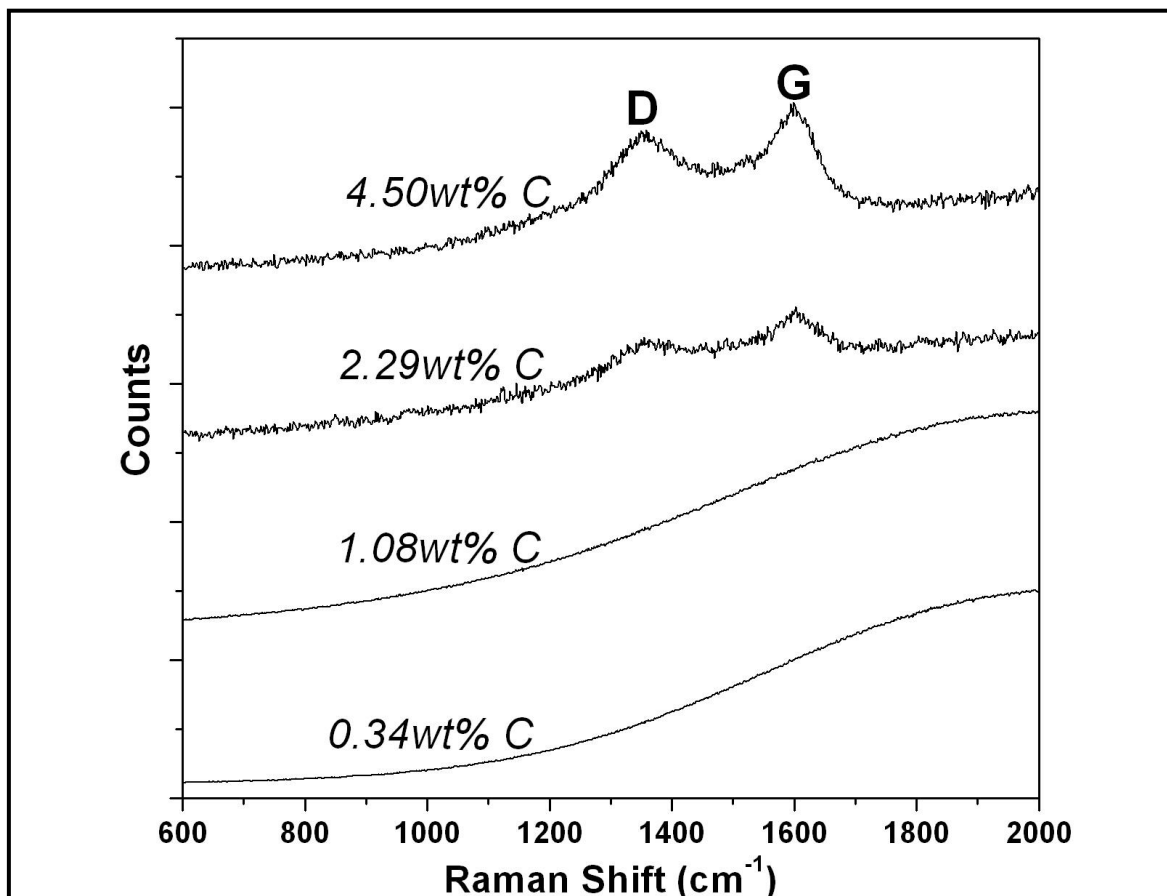


Figure 3.15 Raman spectra obtained from the carbon black - silica aerogel composites showing the emergence of the D (sp^3) and G (sp^3) band peaks with increasing carbon content

We note that there is no signature from the carbon black in the IR transmittance spectra because such homo-nuclear molecules/materials do not exhibit the required dipole moment. Such materials can, however, be evaluated using Raman IR spectrometry, which exploits the variation in molecular polarizability. The Raman spectra obtained from the composite samples with different carbon contents are shown in Figure 3.15. There are no measurable peaks in the spectra obtained from the 0.34 and 1.08 wt.% carbon composites, but in the samples with 2.29 and 4.50 wt.% carbon there are distinct peaks at wave-numbers of 1350 cm^{-1} and 1580 cm^{-1} : these correspond to the D-band (sp^3) and G-band (sp^2), respectively. The areas under these peaks (ID and IG, respectively) were measured by fitting them to a Gaussian-Lorentzian mixture. The clearest peaks were observed for the 4.50 wt.% C composite and in this case the characteristic IG/ID ratio was ~ 0.48 : we note that this lies well within the range of values for typical carbon blacks.

Chapter 4

CONCLUSIONS

Monolithic and transparent silica aerogels were synthesized before the composite aerogel experiments. Two parameters were changed one of them being the TEOS concentration and other one being the aging solutions and temperatures in order to optimize these parameters for further composite studies. Drying of the gels was performed using supercritical carbon dioxide extraction method. Drying procedure simulations were performed and the best conditions were determined considering both the simulations and practical reasons.

It was shown that TEOS concentration had a strong effect on density of the aerogels. It changed the pore sizes and pore volumes significantly as a result of the large differences in the shrinkage values of the samples having different TEOS concentration. However without aging, the gels did not have high porosities and high transparencies for effective thermal insulation. Aging experiments were performed by 60 wt% samples having high porosity and low average pore diameter which leads to low thermal conductivity. It was observed that water was a very effective aging solvent to strengthen the gel structure and decrease shrinkage. The aged samples had higher average pore diameters and their pore volumes were increased significantly.

Once the pore properties are optimized using the sol-gel parameters composite materials of carbon black-silica aerogel were synthesized. The aim of this part is to supply fundamental information for literature about the changes of pore properties of opacified silica aerogels. Carbon black powder mixed with ethanol was added to the sol just after the base catalyst addition. 50 wt% TEOS concentrated gel was used in this part of the study to be able to have enough time for mixing with carbon black before gelation occurs. Monolithic carbon black – silica aerogel composites having the carbon black compositions from 0.34 to 4.5 wt% were produced without sacrificing from high pore volumes and high

surface areas which is very important for high temperature insulation applications. Also IR spectra of the composite samples showed that the chemical structure is not disturbed with carbon addition. This is another advantage for having the desired properties of silica aerogels and eliminating the disadvantages of being fragile and disability of high temperature insulation with carbon addition. The resulting material is a monolithic IR opacified composite aerogel having the advantages of better mechanical properties and lower thermal conductivities than silica aerogels at high temperatures.

BIBLIOGRAPHY

-
- [1] K.I. Jensen, Passive solar component based on evacuated monolithic silica aerogel , *J. Non-Cryst. Solids* , 145, (1992), 237
- [2] G. G.M.Pajonk, E.Elaloui, B. Chevalier, R.Begag, Optical transmission properties of silica aerogels prepared from polyethoxydisiloxanes , *J. Non-Cryst. Solids*, 210, (1997), 224
- [3] B.E.Yoldas, M.J.Annen, J.Bostaph, Chemical engineering of aerogel morphology formed under nonsupercritical conditions for thermal insulation , *Chem. Mater.*,12, (2000), 2475
- [4] Fricke, J.; Lu, X.; Wang, P.; Buttner, D.; Heinemann, U. *Science*, 255, (1992), 2308
- [5] Hrubesh, L. W.; Pekala, R. W., Thermal properties of organic and inorganic aerogels , *J. Mater. Res.*, 9, (1994), 731
- [6] G.M. Pajonk, Transparent silica aerogels , *J. Non-Cryst. Solids*, 225, (1998), 307
- [7] Brinker, C.J. Brinker, K.D. Keefer, D.W. Schaefer, C.S. Achley, Sol-gel transition in simple silicates , *J. Non-Cryst.Solids*, 48 (1982), 47
- [8] C.J. Brinker, K.D. Keefer, D.W. Schaefer, R.A. Assink, B.D. Kay, C.S. Ashley, Sol-gel transition in simple silicates II , *J. Non-Cryst.Solids*, 63, (1984), 45
- [9] G.A. Nicholson, S.J. Teichner, *Bull. Soc. Chim. Fr.*, 5 (1968), 1906
- [10] W.J. Schmitt, MSc thesis, University of Wisconsin Madison, (1982)
- [11] Tag der wissenschaftliche Aussprache : 26. August (2002)
- [12] Brinker, C.J. Brinker, K.D. Keefer, D.W. Schaefer, C.S. Achley, Sol-gel transition in simple silicates , *J. Non-Cryst.Solids*, 48 (1982), 47
- [13] B . Karmakar, G. De, D. Ganguli, Dense silica microspheres from organic and inorganic acid hydrolysis of TEOS , *J. Non-Cryst. Solids*, 272, (2000), 11
- [14] G.W. Sherer, Mechanics of syneresis I. Theory , *J.Non-Cryst.Solids*, 108, (1989), 18
- [15] M. Stolarski, J. Walediewski, M. Steininger, B. Pniak, Synthesis and characteristic of silica aerogels , *Applied Cat. A*, 177, (1999), 139
- [16] Larry L. Hench, Rodrigo Orefice, Sol-gel Technology. In Kirk-Othmer, *Encyclopedia of Chemical Technology*, (2000)

-
- [17] S. Smitha, P. Shajesh, P.R. Aravind, S. Rajesh Kumar, P. Krishna Pillai, K.G.K. Warriar, Effect of aging time and concentration of aging solution on the porosity characteristics of subcritically dried silica aerogels , *Microporous and Mesoporous Materials*, 91, (2006), 286
- [18] Juncal Estella, Jesu s C. Echeverri a, ariano aguna, Julia n J. arrido, Effects of aging and drying conditions on the structural and textural properties of silica gels , *Microporous and Mesoporous Materials*, 102, (2007), 274
- [19] Arnaud Rigacci, Mari-Ann Einarsrud, Elin Nilsen, Rene Pirard, rancoise Ehrburger-Dolle, Bruno Chevalier, mprovement of the silica aerogel strengthening process for scaling-up monolithic tile production , *Journal of Non-Crystalline Solids*, 350, (2004), 196
- [20] G. Reichenauer, Thermal aging of silica gels in ater , *J. Non-Cryst. Solids*, 350, (2004), 189
- [21] Pinnavaia, T. J., *Access in nanoporous materials* , Kluwer Academic Publishers, 1996
- [22] F. Kirkbir, H. Murata, D. Meyers, S. Chaudhuri, Drying of aerogels in different solvents between atmospheric and supercritical pressures , *J.Non-Cryst.Solids* 225, (1998), 14
- [23] P.H. Tewari, A.J. Hunt, K.D. Lofftus, Ambient-temperature supercritical drying of transparent silica aerogels , *Mater. Lett.* 3, (1985), 363
- [24] Hajime Tamon, Taketo Kitamura, Morio Okazaki, Preparation of Silica Aerogel from TEOS , *Journal of Colloid and Interface Science*, 197, (1998), 353
- [25] G.M. Pajonk, Transparent silica aerogels , *Journal of Non-Crystalline Solids*, 225, (1998), 307
- [26] R. Deshpande, D.W. Hua, D.M. Smith, C.J. Brinker, Pore structure evolution in silica gel during aging/drying. III. Effects of surface tension , *J. Non-Cryst. Solids*, 144, (1992), 32
- [27] F. Schwertfeger, D. Frank, M. Schmidt , Hydrophobic waterglass based aerogels without solvent exchange or supercritical drying , *J.Non-Cryst.Solids*, 225, (1989), 18
- [28] F. Schwertfeger, A. Zimmermann, H. Krempel, WO 96/25850, issued 1996
- [29] A.Venkateswara Rao,G.M. Pajonk,S.D. Bhagat,Philippe Barboux, ependence of monolithicity and physical properties of TMOS silica aerogels on gel aging and drying conditions , *J. Non-Cryst. Solids* 350, (2004), 216
- [30] E.Hümmer, X. u, Th. Rettelbach, J. Fricke, Heat transfer in opacified aerogel powders , *J. Non-Cryst. Solids*, 145, (1992), 211
- [31] D. M. Smith, A. Maskara, U. Boes, Aerogel-based thermal insulation , *J. Non-Cryst. Solids* 225, (1998), 254

-
- [32] K.E. Parmenter, F. Milstein, Mechanical properties of silica aerogels , *J. Non-Cryst. Solids*, 223, (1998), 179
- [33] M. Moner-Girona, E. Martinez, A. Roig, J. Esteve, E. Molins, Mechanical properties of silica aerogels measured by microindentation: influence of sol-gel parameters and carbon addition , *J. Non-Cryst. Solids*, 285, (2001), 244
- [34] Christine John Geankoplis, *Transport Process and Separation Process Principles* , Pearson Education, Inc., New Jersey, 2003
- [35] Vafai, Kambiz. *Handbook of Porous Media* , New York, NY, USA: Marcel Dekker Incorporated, 2000.
- [36] W.H. Tao, H.C. Hsu, C.C. Chang, C.L. Hsu, Y.S. Lin, *J. Cell. Plast.*, 37, (2001), 310
- [37] Reim , Korner , anara J, Silica aerogel granulate material for thermal insulation and daylighting , *Solar Energy*, 79, (2005), 131
- [38] G. Q. Lu, X.S. Zhao, *Nanoporous Materials Science and Engineering* , Imperial Collage Press, London, UK, 2004
- [39] Duong D. Do, *Adsorption Analysis: Equilibria and Kinetics* , Imperial Collage Press, London, UK, 1998
- [40] T. Funazukuri, C.Y. Kong, S. Kagei, Impulse response techniques to measure binary diffusion coefficients under supercritical conditions , *J. Chromatogr, A* 1037, 2004, 411-429
- [41] Ralph T. Yang, *Adsorbents: Fundamentals and Applications* , John Wiley & Sons, Inc, Hoboken, New Jersey, 2003
- [42] Peter J., Taylor & Francis, Limited, London, New York, 2000